Mathematical Biosciences and Engineering

http://www.aimspress.com/journal/MBE

MBE, 16(6): 7616–7658.
DOI: 10.3934/mbe.2019382
Received: 28 March 2019
Accepted: 11 August 2019
Published: 20 August 2019

Research article

Mathematical investigation of HBeAg seroclearance

Sarah Kadelka and Stanca M Ciupe*

Department of Mathematics, Virginia Polytechnic Institute and State University, Blacksburg, VA 24061, USA

* **Correspondence:** Email: stanca@vt.edu; Tel: +15402313190.

Abstract: Spontaneous or drug-induced loss of hepatitis B e antigen is considered a beneficial event in the disease progression of chronic hepatitis B virus infections. Mathematical models of within-host interactions are proposed; which provide insight into hepatitis B e antibody formation, its influence on hepatitis B e antigen seroclearance, and reversion of anergic cytotoxic immune responses. They predict that antibody expansion causes immune activation and hepatitis B e antigen seroclearance. Quantification of the time between antibody expansion and hepatitis B e antigen seroclearance in the presence and absence of treatment shows that potent short-term treatment speeds up the time between antibody expansion and hepatitis B e antigen seroclearance. The monthly hepatocyte turnover during this time can be increased or decreased by treatment depending on the amount of core promoter or precore mutated virus produced. The results can inform human interventions.

Keywords: hepatitis B; HBeAg; HBeAb; seroclearance; mathematical modeling

1. Introduction

Hepatitis B virus (HBV) infection is a major public health burden with high endemic areas in South East Asia, China, and sub-Saharan Africa [1]; and approximately 240 million chronically infected people worldwide [2]. HBV infects a subset of liver cells (*i.e.* hepatocytes) [3] and can lead to either acute or chronic disease. About 90% of perinatally and 20-30% of childhood acquired HBV infections become chronic [4], while healthy adults clear the infection in 95% of the cases [3]. Severe complications, such as liver cirrhosis and hepatocellular carcinoma (HCC), follow chronic infections [3].

Chronic HBV spans five distinct disease stages which are built around the dynamics of a serological marker called hepatitis B e antigen (HBeAg), a secretory protein that is not required for viral replication or hepatocyte infection [5] and has been described as a downregulator of the cellular immune response, therefore acting as an immune tolerogen [6]. The stages are not clearly separated

or sequential [2]. The first four are distinguished by the presence/absence of HBeAg and by disease (hepatitis), as described below [2]. The first phase, called HBeAg-positive infection (formerly known as the immune tolerant phase), lasts between 10–30 years [2, 4]. Viral DNA levels are high and HBeAg is detectable, while alanine aminotransferase (ALT) (a marker of liver disease) is normal, indicating lack of liver cell damage [4, 7]. The second stage, called HBeAg-positive hepatitis (formerly known as immune clearance or immune active phase), is characterized by high and fluctuating viral DNA levels, the presence of HBeAg, elevated ALT and moderate to severe liver damage [2, 4]. The third phase, called HBeAg-negative infection phase (formerly the inactive carrier phase), is marked by HBeAg seroconversion, *i.e.* hepatitis B e-antibody (HBeAb) production and subsequent HBeAg loss, low viral DNA levels, normal ALT and no liver disease [2, 8]. The fourth phase, called HBeAg-negative hepatitis, is characterized by undetectable HBeAg, detectable HBeAb, moderate to high viral DNA levels, elevated ALT and liver disease [2]. The fifth phase, which is no longer determined by HBeAg, is called hepatitis B surface antigen (HBsAg) negative phase. It is marked by normal ALT levels and usually undetectable viral DNA levels [2]. Reaching this phase before the onset of cirrhosis significantly reduces the risk of liver damage (either by cirrhosis or HCC) [2].

For chronically infected HBV patients two main groups of HBV drugs are available: interferon-α (IFNα) or its pegylated form PegIFNα, and five nucles(t)ide analogues (NAs): lamivudine, telbivudine, adefovir, entecavir, and tenofovir [9]. IFNs have both immunoregulatory and antiviral effects [9]. NAs have only antiviral effects, such as inhibition of HBV replication [9, 10]. The goal of HBV treatment is to reduce the risk of disease progression and HCC development [2]. The optimal treatment endpoint is seroclearance of HBsAg, associated with a very low risk of viral relapse and progression to HCC [2, 11].

The severe side effects associated with IFNα and PegIFNα limit the amount of time when they can be administrated: usually 48 weeks, but in certain cases up to 96 weeks [2, 12]. Therefore, the more widely used treatment options are NAs. Older NAs caused viral resistance, but this risk was significantly reduced by the newest generation of NAs: entecavir and tenofovir, which allow for long-term (indefinite) treatment [2, 13–15]. In spite of these advances in NAs therapy, HBsAg seroclearance is reached in only 1% of treated patients [13]. Hence HBeAg seroconversion, in addition to viral remission to an undetectable viral DNA level, is often considered a more realistic treatment endpoint [11, 16]. In particular, for HBeAg-positive patients that undergo HBeAg seroconversion and viral remission during treatment, stopping therapy after some consolidation phase is recommended [2]. A systematic review of NA treatment studies has reported that after initial seroconversion about 95 (92, 88)% of patients stay HBeAg-negative for 6 (12, 24) months post treatment cessation, and that about 73 (62, 53 51)% of initially HBeAg-positive patients remain in viral remission 6 (12, 24, 36) months after the end of therapy. [13].

The role of HBeAg seroconversion has been investigated in several clinical studies. It has been reported that patients that undergo HBeAg seroconversion have a better prognosis than those that are consistently seropositive, such as slower disease progression and regression of the fibrosis [17, 18]. Other studies have shown that persistently HBeAg-positive patients have a higher risk of developing HCC [19], and liver cirrhosis [20–22]. Additionally prolonged HBeAg-positive hepatitis or higher age at HBeAg seroconversion was associated with a higher risk for liver cirrhosis [21, 23–25].

Drug therapy was correlated with faster HBeAg seroconversion. A meta-analysis reported increased

HBeAg seroconversion rates after one year of NA treatment regardless of NAs efficacy [26]. Another meta-analysis reported that the rates of HBeAg seroconversion after one year of treatment are greatest for tenofovir [27] and telbivudine [28]. However, for longer treatment periods (of 3,4,5 years) the rate of HBeAg seroconversion is reduced compared to spontaneous seroconversion obtained without treatment [28, 29], indicating that a prolonged duration of treatment with, in particular the highly efficient NAs entecavir and tenofovir, is deleterious in achieving HBeAg seroconversion. Given the importance of HBeAg in HBV pathogenesis and the contradictory reports regarding spontaneous and drug-induced HBeAg seroconversion, we propose a mathematical modeling approach for studying the dynamics of HBeAg loss under various hypotheses. The developed models will investigate the role of antibody formation, their role in the disease transition from HBeAg-positive to HBeAg-negative infections, and the trade-off between virus loss during therapy and HBeAg seroclearance.

Over the past decades, mathematical models have been developed to study the dynamics of acute, chronic, and occult HBV infections [30–32], drug therapy [33–41], cell-to-cell transmission [42], intracellular interactions [42–44], cellular immune responses [31, 34, 45–47], antibody-mediated immune responses [44, 48, 49], HBeAg [44, 50], and HBeAb [44]. We build on the previous modeling work and consider the interaction between HBeAg, cellular immune responses, HBeAb levels and drug efficacy. We hypothesize that B cells mature into HBeAb-producing plasma cells during the HBeAg-positive stages of HBV infection, investigate various modulation mechanisms for HBeAb dynamics, and use the models to predict the differences in seroconversion times under treatment and in the absence of treatment.

This paper is structured as follows. In Section 2, we develop an in-host model of hepatitis B infection in the absence of therapy which focuses on the function of HBeAg in disease progression. In Section 3, we investigate the model analytically and numerically and predict the interplay between cellular and antibody responses on HBeAg seroclearance. In Section 4, we investigate the role of NAs treatment on HBeAg seroclearance. We conclude with a discussion.

2. Model development

We model the interactions between uninfected hepatocytes, T; infected hepatocytes, I; hepatitis B virus, V; effector cytotoxic T lymphocytes (CTLs), E; HBeAg, e; HBeAb, A; and HBeAg-HBeAb immune complexes, X. To incorporate the ability of the liver to regenerate after cell loss [51], we assume that uninfected hepatocytes follow a logistic growth with maximum proliferation rate r and carrying capacity T_m. They become infected with HBV at rate β. Infected hepatocytes are killed by effector cells at rate μ, and produce virus and HBeAg at rates p and π, respectively. Furthermore, we assume that infected cells proliferate with maximum proliferation r [32, 37, 45]. Since there is evidence, at least in acute HBV infections [32, 45, 52], that covalently closed circular DNA can be lost during cell proliferation, we assume that an infected cell produces one uninfected and one infected offspring. HBV is cleared at rate c. Effector cells are recruited at constant rate s_E and, after interaction with infected cells, expand at maximum rate α and carrying capacity E_m [46]. It has been reported that HBeAg suppresses the cellular immune responses [6, 53]. We model this by decreasing the effector cell recruitment at rate σ. Effector cells die at rate d_E. We only model the cytolytic effect of the effector cells and ignore their non-cytolytic function [31]. HBeAgs decay at per capita rate δ_e and bind HBeAb to form complexes at rate k_p. Complexes dissociate at rate k_m and decay at per capita rate

$c_X = \delta_e + d_X$, where δ_e is the decay rate of HBeAg and d_X is increased removal due to phagocytosis. Previous papers [54] have presented detailed models of B lymphocyte proliferation and differentiation into plasmablast, antibody producing plasma cells and memory cells after they encounter antigen. For simplicity, we ignore the details of B-lymphocyte dynamics and differentiation into antibody producing cells and assume that free HBeAb, A, is produced at rate s proportional to the HBeAg. Moreover HBeAb is maintained after HBeAg clearance through antigen-independent homeostatic proliferation of memory B cells and long-lived plasma cells, which we model through a logistic term with maximum proliferation rate s_A and carrying capacity A_m [49]. The corresponding system of equations is given by system (2.1) and a schematic representation is shown in Figure 1.

$$\begin{aligned}
\frac{dT}{dt} &= r(T+I)\left(1-\frac{T+I}{T_m}\right)-\beta TV,\\
\frac{dI}{dt} &= \beta TV-\mu IE,\\
\frac{dV}{dt} &= pI-cV,\\
\frac{de}{dt} &= \pi I-\delta_e e-k_p Ae+k_m X,\\
\frac{dE}{dt} &= \frac{s_E E+\alpha IE}{1+\sigma e}\left(1-\frac{E}{E_m}\right)-d_E E,\\
\frac{dA}{dt} &= (s_A A+seA)\left(1-\frac{A}{A_m}\right)-k_p Ae+k_m X,\\
\frac{dX}{dt} &= k_p Ae-k_m X-(\delta_e+d_X)X.
\end{aligned} \tag{2.1}$$

All parameters in this model are positive. Moreover the initial conditions are

$$T(0)=T_0, I(0)=I_0, V(0)=V_0, e(0)=e_0, E(0)=E_0, A(0)=A_0, X(0)=X_0.$$

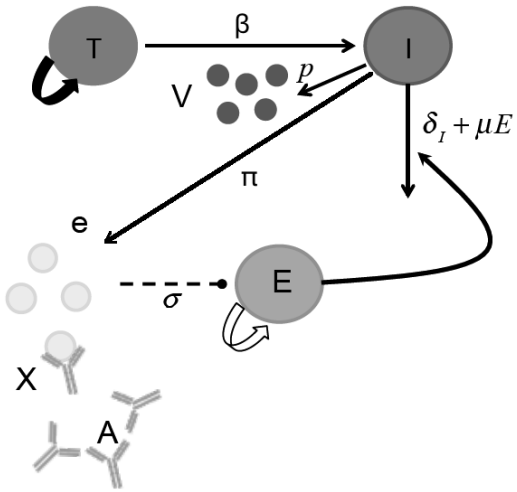

Figure 1. Model schematic including interactions given in system (2.1). Solid lines describe up-regulation or production and dashed lines describe inhibition.

3. Results

3.1. Analytical results

System (2.1) has four virus clearance equilibria. Equilibrium $S_2 = (T_m, 0, 0, 0, 0, 0, 0)$ where clearance happens in the absence of immune responses, equilibrium $S_4 = \left(T_m, 0, 0, 0, \frac{E_m(s_E - d_E)}{s_E}, 0, 0\right)$ where clearance is achieved due to CTL responses, and equilibrium $S_8 = (T_m, 0, 0, 0, 0, A_m, 0)$ where HBeAb responses are maximal and CTL responses are absent are unstable. Lastly, equilibrium $S_{10} = \left(T_m, 0, 0, 0, \frac{E_m(s_E - d_E)}{s_E}, A_m, 0\right)$ where CTL responses are present and HBeAb responses are maximal is locally asymptotically stable when $(T_m \beta p s_E)/(E_m \mu c(s_E - d_E)) < 1$ and $s_E > d_E$. This means that when virus and infected cells are cleared faster than produced, while CTLs are produced faster than cleared, infection dies out.

Similarly, positive virus equilibria can be obtained in the absence of any immune responses (S_5), in the presence of anergic CTL responses (S_6), under positive but inefficient antibody responses (S_{11}), and in the presence of both anergic CTLs and inefficient antibody responses (S_{12}). The exact description of these equilibria, other equilibria that are not mentioned here, and their stability can be found in the supplementary material (Appendix 1).

3.2. Numerical results

3.2.1. Parameter values

The parameter values used in the simulations are given in Table 1. Liver makes up one fiftieth of a persons weight [55]. Each gram of liver contains 14×10^7 hepatocytes [56]. Therefore, an average 70 kg person has about 2×10^{11} hepatocytes. As in [45], distributing this throughout 15L of extracellular fluid results in a liver capacity of $T_m = 13.6 \times 10^6$ hepatocytes/mL.

Liver cells have the potential to regenerate fast. We account for it by setting the hepatocyte proliferation rate to $r = 1$/day, as in [31, 49]. The estimates for the infected hepatocytes' half-lives range between 10–100 days [30]. Given that we assume a maximum effector cells' level of $E_m = 10^3$ cells/mL, and an infected hepatocytes' half-life of 11 days, the infected cells clearance rate becomes $\mu = \ln 2/(11 \times E_m) = 6 \times 10^{-5}$ mL/(cells×day). The estimates for virus' half-life is at most 4.4 hours [57]. We assume a half-life of 4 hours, corresponding to a decay rate of $c = 4.2$/day. The viral infectivity rate during acute HBV infection was estimated to range between $10^{-10} - 1.8 \times 10^{-9}$ mL/(virus×day) [49] and the virus production rate ranges between 200–1000/day [58]. Since virus levels are lower during chronic disease, we consider a one-fold reduction in the infectivity rate $\beta = 4 \times 10^{-11}$ mL/(virus×day) and keep the viral production levels as in acute cases, $p = 400$/day. Similar results can be obtained for high (acute level) infectivity and reduced production rates (not shown). As in [50], we assume that HBeAg is degraded at rate $\delta_e = 0.3$/day. The half-life of effector cells is short, therefore we assume a decay rate of $d_E = 0.5$/day [47, 50, 59].

The dissociation rate of HBsAg-HBsAb immune complexes is $k_m = 10$/day [49]. We assume the same is true for HBeAg-HBeAb dissociation rate. Furthermore, we assume that HBeAb is mostly IgG and that the avidity for HBeAg-HBeAb binding is similar to that for HBsAg-HBsAb binding, which is set at $K = 10^7 \mathrm{M}^{-1}$ as in [60]. For an IgG molecular weight of 150kDa = 150×10^3g/mol [49], and a

conversion of 1 IgG in mg/mL = 13.43 IgG in IU/mL [61], we obtain a binding rate

$$\begin{aligned} k_p = k_m \times K &= 10^8 \frac{1}{\mathrm{M} \times \mathrm{d}} = \frac{10^8 \mathrm{L}}{\mathrm{mol} \times \mathrm{d}} = \frac{10^8 \mathrm{L}}{\mathrm{mol} \times \mathrm{d}} \times \frac{1000 \mathrm{mL}}{\mathrm{L}} \times \frac{\mathrm{mol}}{150 \times 10^3 \mathrm{g}} \\ &= \frac{10^8}{150} \times \frac{\mathrm{mL}}{\mathrm{d} \times 10^3 \mathrm{mg}} = \frac{10^5}{150} \times \frac{1}{\mathrm{d}} \times \frac{\mathrm{mL}}{\mathrm{mg}} = \frac{10^5}{150 \times 13.43} \times \frac{\mathrm{mL}}{\mathrm{IU} \times \mathrm{d}} \\ &\approx 50 \times \frac{\mathrm{mL}}{\mathrm{IU} \times \mathrm{d}}. \end{aligned} \tag{3.1}$$

The remaining parameters are chosen as follows. We assume that infected cells produce HBeAg at rate $\pi = 10^{-4}$ IU/(cells×day), and activate effector cells at rate $\alpha = 2.1$/(cells×day). Further, effector cells are activated in an infected cell independent manner at rate $s_E = 0.1$/day and their production is inhibited by HBeAg at rate $\sigma = 10^4$ mL/IU. HBeAb is produced in an HBeAg-independent manner at rate $s_A = 10^{-10}$/day and has a carrying capacity of $A_m = 10$ IU/mL. HBeAg-dependent HBeAb production rate s will be varied throughout our investigations. Lastly, the HBeAg-HBeAb immune complex removal rate is $c_X = 1.2$/day, four times higher than the clearance of free HBeAg [62].

3.2.2. Initial conditions

While free HBeAb is not detected by assays during most chronic HBeAg-positive HBV infections, it is reasonable to believe that antibody specific for HBeAg are present in immune complexes before the free antibody can be detected. This has been shown in HIV infections where immune complexes have been detected three weeks prior to free antibody detection [63]. However, since the number of immune complexes is small, we model this by assuming HBeAb is initially negligible, *i.e.* $A = 0$, and $X = 0$. Under this assumption HBeAb does not influence the dynamics of the remaining variables and system (2.1) reduces to

$$\begin{aligned} \frac{dT}{dt} &= r(T+I)\left(1 - \frac{T+I}{T_m}\right) - \beta T V, \\ \frac{dI}{dt} &= \beta T V - \mu I E, \\ \frac{dV}{dt} &= pI - cV, \\ \frac{de}{dt} &= \pi I - \delta_e e, \\ \frac{dE}{dt} &= \frac{s_E E + \alpha I E}{1 + \sigma e}\left(1 - \frac{E}{E_m}\right) - d_E E. \end{aligned} \tag{3.2}$$

Furthermore, during HBeAg-positive infection, the CTL immune responses are suppressed. We model this by assuming an immune tolerant equilibrium, in which the CTL responses are non-existent or reduced. Asymptotic analysis of model (3.2) (see supplementary material, Appendix 1) shows that there are at most five equilibria in which virus population is non-zero: a no CTL state in which the entire liver is infected

$$S_5^{noA} = \left(0, T_m, \frac{T_m p}{c}, \frac{T_m \pi}{\delta_e}, 0\right) \tag{3.3}$$

and at most four CTL-inefficient infectious states

$$S_6^{noA} = \left(\bar{T}(\bar{I}), \bar{I}, \frac{p}{c}\bar{I}, \frac{\pi}{\delta_e}\bar{I}, \bar{E}(\bar{I})\right), \tag{3.4}$$

where

$$\bar{T}(\bar{I}) = \frac{((\alpha\delta_e - \pi\sigma d_E)\bar{I} + \delta_e(s_E - d_E))E_m c\mu}{\delta_e\beta p(\alpha\bar{I} + s_E)},$$

$$\bar{E}(\bar{I}) = \frac{((\alpha\delta_e - \pi\sigma d_E)\bar{I} + \delta_e(s_E - d_E))E_m}{\delta_e(\alpha\bar{I} + s_E)},$$

and $\bar{I}$ is a root of the fourth degree polynomial

$$C_4\bar{I}^4 + C_3\bar{I}^3 + C_2\bar{I}^2 + C_1\bar{I} + C_0. \tag{3.5}$$

The coefficients C_0, C_1, C_2, C_3, and C_4 are defined in Appendix 1.

Equilibrium S_5^{noA} represents completely absent CTL responses, while S_6^{noA} represents inefficient (exhausted) CTL responses. Studies have shown that during chronic HBeAg-positive infections, cellular immune responses are anergic rather than completely absent [64]. We therefore assume that the equilibrium in the absence of HBeAb is given by S_6^{noA}, where the CTL responses are non-zero but inefficient. Numerically we find that this is the only stable equilibrium of system (3.2) for the parameter values given in Table 1. Our goal is to investigate how the emergence of antibodies affects HBeAg dynamics and how much this event contributes to the reverting of T cell exhaustion. To address this, we investigate the dynamics of system (2.1) under initial conditions given by the T cell exhaustion state (3.4), together with a small initial free HBeAb concentration $A_0 = 10^{-6}$ IU/mL. This means that at time $t = 0$ we perturb system (2.1) from its unstable equilibrium $(S_6^{noAb}, 0, 0)$ by introducing a small number of free HBeAb. These initial conditions are summarized in Table 2.

Table 1. Parameter values.

Parameter	Description	Value	Unit	References
r	proliferation rate of hepatocytes	1	d^{-1}	[31, 49]
T_m	hepatocyte carrying capacity	13.6×10^6	cells/mL	[45, 55, 56]
p	virus production rate	400	mL/(virus×d)	[58]
c	virus clearance rate	4.2	d^{-1}	[57]
δ_e	HBeAg degradation rate	0.3	d^{-1}	[50]
d_E	immune cell death rate	0.5	d^{-1}	[47, 50, 59]
d_X	complex removal rate due to phagocytosis	$3 \times \delta_e$	d^{-1}	
k_p	HBeAb binding rate	50	mL/(IU×d)	see text
k_m	HBeAb dissociation rate	10	d^{-1}	see text
β	viral infectivity rate	4×10^{-11}	mL/(virus×d)	[49], see text
μ	effector induced infected cells clearance rate	6×10^{-5}	mL/(cells×d)	[30], see text
π	e-antigen production rate	10^{-4}	IU/(cells×d)	
α	infected cell dependent immune cell activation rate	2.1	1/(cells×d)	
s_E	infected cell independent immune cell activation rate	0.1	d^{-1}	
σ	strength of e-antigen inhibition	10^4	mL/IU	
E_m	effector cells carrying capacity	10^3	cells/mL	
s	HBeAg dependent HBeAb production rate	*varied*	mL/(IU×d)	
s_A	HBeAg independent HBeAb production rate	10^{-10}	d^{-1}	
A_m	HBeAb carrying capacity	10	IU/mL	

Table 2. Initial conditions with $\bar{T},\ \bar{I},\ \bar{V},\ \bar{e},\ \bar{E}$ as defined in (3.4).

Initial condition	Description	Value	Unit
T_0	target cells	$\bar{T}$	cells/mL
I_0	infected cells	$\bar{I}$	cells/mL
V_0	virus	$\bar{V}$	virus/mL
e_0	HBeAg	$\bar{e}$	IU/mL
E_0	effector cells	$\bar{E}$	cells/mL
A_0	HBeAb	$\begin{cases} 10^{-6}, & \text{(HBeAb expansion)} \\ 0, & \text{(negligent HBeAb)} \end{cases}$	IU/mL
X_0	HBeAg-HBeAb immune complexes	0	IU/mL

3.2.3. The dynamics of HBeAg and CTL populations

For the parameter values in Table 1, and HBeAg-dependent HBeAb production rate $s = 6$ mL/(IU×d), the system's dynamics are shown in Figure 2. The solid and dashed curves show the dynamics in the presence and absence of HBeAbs. If the effects of the HBeAb are negligible, then the HBeAg levels do not change and the CTL responses are not strong enough to cause viral remission (see Figure 2, dashed curves). Contrarily, spontaneous HBeAb production leads to virus suppression below the threshold level of HBeAg-negative infections, corresponding to 10^4 cp/mL [11], which for the remainder of our study will be called *low level virus concentration*. The HBeAg population drops below 0.1 IU/mL, corresponding to the lower limit for HBeAg quantification assays, which for the remainder of our study will be called *HBeAg seroclearance* level (see Figure 2, solid curves).

We investigated which immune factors are responsible for HBeAg seroclearance, as well as for the infected cells' decay. Both HBeAg and infected cells decrease in biphasic manner (see Figure 3). The first slope decay is steeper for HBeAg than for infected cells, while the second slope decays are the same (see Figure 3, grey versus black lines). The additional removal of free HBeAg during the first phase decay is due to antibody binding, and the formation and removal of immune-complexes by phagocytes. Following the initial antibody responses, a decrease in HBeAg levels leads to a decrease in their tolerogenic pressure on CTLs, which get activated and kill infected cells. As a result, infected cells do get removed by potent cellular immune responses, but HBeAg production slows down as well. During the second phase decay, CTL responses outweigh the antibody responses, hence, the slopes for both HBeAg and infected cells' decay are identical.

Together, this analysis leads to the prediction that a combination of antibody and cellular responses is needed to drive the system into a state of low level virus concentration and undetectable HBeAg. Antibody responses act first, by reducing the immune tolerant effects of HBeAg, while cellular responses control the later stages of the infection.

As shown in Figure 2, under HBeAb responses which grow in an HBeAg-dependent manner at rate $s = 6$ mL/(IU×d), HBeAg is cleared in 2.8 years. We quantified the time of HBeAg seroclearance, $\tau(s)$, as a function of the HBeAb production rate s for $5.51 \leq s \leq 50$ mL/(IU×d) (see Figure 4). For $s < 5.51$ mL/(IU×d), HBeAg seroclearance is never reached. The time to HBeAg seroclearance

(below 0.1 IU/mL) decreases from 41.9 years for small $s = 5.51$ mL/(IU×d) to 1.2 years for $s > 50$ mL/(IU×d) (see Figure 4). As expected, higher antibody expansion rates lead to shorter times to HBeAg seroclearance. The time to HBeAg seroclearance is dependent on the initial HBeAb level, with faster HBeAg clearance for high initial HBeAb levels (see Figure S1). In our simulations we fixed $A_0 = 10^{-6}$ IU/mL to avoid any numerical problems.

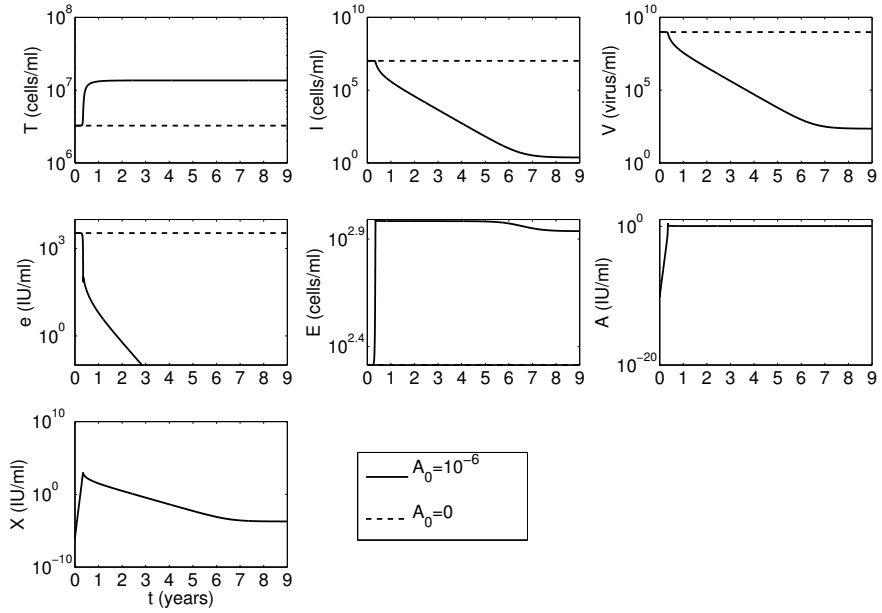

Figure 2. The dynamics of the system (2.1) when $A_0 = 10^{-6}$ IU/mL (solid lines) and $A_0 = 0$ IU/mL (dashed lines). Here, $s = 6$ mL/(IU×d) and all other parameters are given in Table 1.

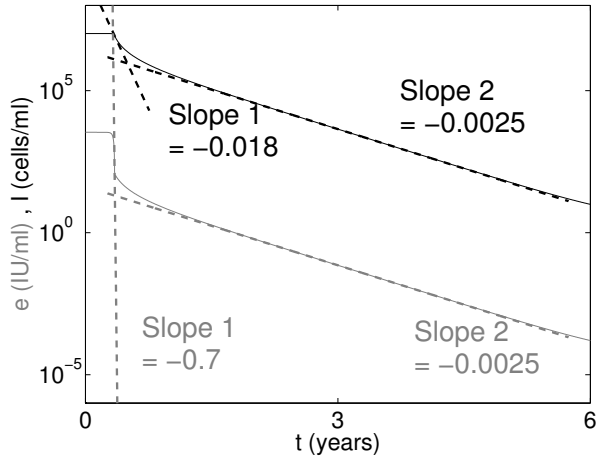

Figure 3. Dynamics of the infected cells (black) and HBeAg (grey) as given by (2.1), together with the estimated slopes of decay. Here $A_0 = 10^{-6}$ IU/mL, $s = 6$ mL/(IU×d), and all other parameters are given in Table 1.

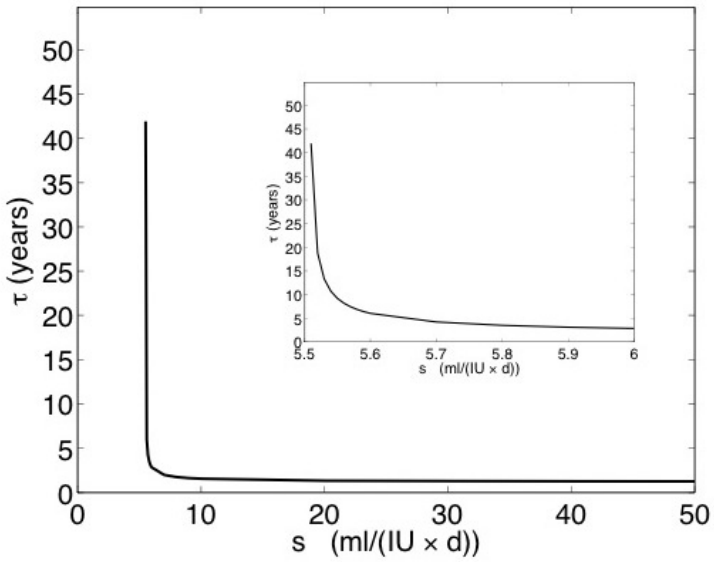

Figure 4. HBeAg seroclearance time versus HBeAb production rate s when $A_0 = 10^{-6}$ IU/mL.

3.3. Core and precore mutations

Host-virus predictors for HBeAg seroconversion are limited, especially in chronic infections with high virus loads [65]. Two positive events that lead to HBeAg loss are virus mutations in the core promoter [66] and precore region [67], which prevent the coding of HBeAg and lead to loss of HBeAg-positive virus. Clinical studies have found that at least one core/precore mutation can be found in 89% of HBeAg-negative patients and 56% of HBeAg-positive patients [68]. Another study [69] has reported even higher numbers of HBeAg-positive patients with core/precore mutations. We, therefore, assume that core/precore mutations precede the HBeAg seroclearance. However, the quantitative relationship between mutation rates and time to HBeAg seroconversion is not known. Core/precore mutations in our investigations can be seen as a proxy for any event leading to an infected cell's loss of HBeAg production. Here, we investigate the role of mutations in HBeAg clearance as follows. We modify system (2.1) to include both wildtype HBeAg-positive virus V_w, and mutant HBeAg-negative virus V_m. Cells are either infected by wiltdtype or mutant viruses, I_w and I_m. At time t_1, a fraction Φ of the viruses produced by I_w are HBeAg-negative and the rest $1 - \Phi$ are HBeAg-positive. We ignore back mutations based on the observation that HBeAg-negative virus is mostly inactive. By contrast, all viruses produced by I_m are HBeAg-negative. Wildtype and mutant viruses replicate at rates p_w and p_m, and are cleared at rates c_w and c_m. Furthermore, hepatocytes get infected by wildtype and mutant viruses at rates β_w and β_m and are killed by CTLs at rates μ_w and μ_m. We assume that during division an infected hepatocyte of either wild or mutant-type (I_w or I_m) produces one uninfected and one infected offspring of the same hepatocyte type. The system describing these interactions is

$$
\begin{aligned}
\frac{dT}{dt} &= r(T + I_w + I_m)\left(1 - \frac{T + I_w + I_m}{T_m}\right) - \beta_w T V_w - \beta_m T V_m,\\
\frac{dI_w}{dt} &= \beta_w T V_w - \mu_w I_w E,\\
\frac{dI_m}{dt} &= \beta_m T V_m - \mu_m I_m E,\\
\frac{dV_w}{dt} &= p_w(1 - \Phi(t))I_w - c_w V_w,\\
\frac{dV_m}{dt} &= p_m I_m + p_w \Phi(t) I_w - c_m V_m,\\
\frac{de}{dt} &= \pi I_w - \delta_e e - k_p A e + k_m X,\\
\frac{dE}{dt} &= \frac{s_E E + \alpha(I_w + I_m)E}{1 + \sigma e}\left(1 - \frac{E}{E_m}\right) - d_E E,\\
\frac{dA}{dt} &= (s_A A + seA)\left(1 - \frac{A}{A_m}\right) - k_p A e + k_m X,\\
\frac{dX}{dt} &= k_p A e - k_m X - c_X X,
\end{aligned}
\tag{3.6}
$$

where $\Phi(t) = \begin{cases} 0, & \text{if } t < t_1 \\ \Phi, & \text{if } t \geq t_1 \end{cases}$.

All parameters in this model are positive. Moreover the initial conditions are $T(0) = T_0, I_w(0) = I_0, I_m(0) = 0, V_w(0) = V_0, V_m(0) = 0, e(0) = e_0, E(0) = E_0, A(0) = A_0, X(0) = X_0$, where $T_0, I_0, V_0, e_0, E_0, A_0, X_0$ are defined as in the case of system (2.1).

3.3.1. Analytical results

We assume that the wildtype and mutant viruses are identical in everything but their ability to produce HBeAg, *i.e.* $\beta_w = \beta_m = \beta$, $\mu_w = \mu_m = \mu$, $p_w = p_m = p$, $c_w = c_m = c$, and analyze the long-term behavior of the system. System (3.6) has the following non-infectious equilibria: viral clearance in the absence of antibody responses, $S_2^{mut} = (T_m, 0, 0, 0, 0, 0, 0, 0, 0)$, viral clearance due to CTL responses, $S_4^{mut} = \left(T_m, 0, 0, 0, 0, 0, \frac{E_m(s_E - d_E)}{s_E}, 0, 0\right)$, virus clearance under maximal antibody responses, $S_6^{mut} = (T_m, 0, 0, 0, 0, 0, 0, A_m, 0)$ which are all unstable; and viral clearance in the presence of CTL and maximal antibody responses, $S_8^{mut} = \left(T_m, 0, 0, 0, 0, 0, \frac{E_m(s_E - d_E)}{s_E}, A_m, 0\right)$, which is locally asymptotically stable if and only if $s_E > d_E$ and $\frac{T_m \beta p s_E}{E_m \mu c (s_E - d_E)} < 1$.

The model has two equilibria in which only the mutant virus persists and the wildtype virus goes extinct: mutant persistence in the presence of anergic CTL responses S_{11}^{mut}, which is unstable; and mutant persistence due to a combination of CTL and maximal antibody responses, S_{12}^{mut}. Furthermore, the system has two hyperplanes of equilibria, where HBeAg can take on any value, and in which mutant and wildtype virus coexist: coexistence in the absence of any immune responses, S_9^{mut}, which is biologically relevant if $e < T_m \pi / \delta_e$; and coexistence under antibody responses, S_{10}^{mut}. Coexistence of wildtype and mutant virus results results in infection of the entire liver. For S_9^{mut}, S_{10}^{mut}, and S_{12}^{mut} we did not perform stability analysis (see supplementary material, Appendix 2 for details).

3.3.2. Numerical results

We are interested in the relationship between the time of HBeAg seroclearance and the time of precore/core mutations. First, we want to see how the timing of HBeAg seroclearance under mutation (with and without concomitant free HBeAb expansion) compares with the timing of HBeAg seroclearance in the absence of mutations and presence of antibodies. We plot the dynamics of the total virus in the presence of antibody as given by the system without mutations (2.1) for $s = 6$ mL/(IU×d) and $A_0 = 10^{-6}$ IU/mL (see Figure 5, solid curves) and the dynamics of the wildtype virus given by the system with mutations (3.6) for $\Phi = 0.12$ and $A_0 = 0$ IU/mL (see Figure 5, dashed curves). In both scenarios, HBeAg clearance takes 2.8 years (see Figure 5, HBeAg (e) panel, solid versus dashed curves). Furthermore, if $A_0 = 10^{-6}$ IU/mL at the time of core/precore mutations in system (3.6), HBeAg clearance takes 1.4 years, twice as fast as in either of the single event scenarios (see Figure 5, dotted curves). Additionally, model (3.6) predicts the asymptotic loss of wildtype virus, cells infected with the wildtype virus, HBeAg, and HBeAg-HBeAb immune complexes. The total virus population is reduced from $\bar{V}_{total} = 863.5$ cp/mL in model (2.1) to $\bar{V}_{total} = \bar{V}_n = 161.6$ cp/mL in model (3.6). This is independent of antibody help (see Figure 6).

Clinical studies predicted that initial core/precore mutations are followed by the appearance of antibodies against the HBeAg [70]. We test the effect that the two sequential events, mutations followed by HBeAb expansion, have on HBeAg loss as follows. Let $\tau_1(t_0, \Phi)$ and $\tau_2(t_0, \Phi)$ be the times between spontaneous HBeAb expansion and HBeAg seroclearance when mutations with frequency Φ occur at $t = 0$ and $t = t_0 > 0$. In both cases $A_0 = 10^{-6}$ IU/mL antibodies are introduced at time $t = t_0$ (see Figure 7). In other words, τ_1 measures the time between HBeAb expansion (at time t_0) and HBeAg seroclearance when core/precore mutations start t_0 days before HBeAb expansion (*i.e.* at time 0), while τ_2 measures the time between HBeAb expansion (at time t_0) and HBeAg seroclearance when core/precore mutations and HBeAb expansion start concomitantly at time t_0. Since the system is at equilibrium in the absence of mutations (i.e. in the context of τ_2 from time 0 to t_0), $\tau_2(0, \Phi) = \tau_2(t_0, \Phi) = \tau_1(0, \Phi)$ for all t_0. The difference between the two seroclearance times, $\tau_1(t_0, \Phi) - \tau_2(t_0, \Phi)$, are shown in Figure 8.

We only consider ranges of t_0 and Φ where $\tau_1(t_0, \Phi)$ is positive, based on the assumption that HBeAb expansion happens before HBeAg seroclearance. For any fraction of mutations Φ, we have $\tau_1(0, \Phi) = \tau_2(0, \Phi)$, *i.e.* $\tau_1(0, \Phi) - \tau_2(0, \Phi) = 0$. The model predicts that for $\Phi > 0.1$, as t_0 increases, $\tau_1(t_0, \Phi)$ and consequently $\tau_1(t_0, \Phi) - \tau_2(t_0, \Phi)$ decrease for small and large t_0, and increase for intermediate t_0 values (see Figure 8, right panel, for $\tau_1(0, 0.5) - \tau_2(0, 0.5) = 0$). Very large t_0 values result in HBeAg seroclearance that is exclusively driven by mutations (see Figure 8, white region). For fixed $\Phi < 0.1$, $\tau_1(t_0, \Phi) - \tau_2(t_0, \Phi)$ decreases as t_0 increases leading to $\tau_1 \sim \tau_2$ for small Φ and all t_0 within $0 \leq t_0 < 40$ months.

Hepatocyte turnover. Changes in HBeAg are associated with the activation of adaptive immune responses, fluctuations in HBV DNA and ALT levels, and minimal to high liver damage. Events such as spontaneous HBeAg seroconversion and emergence of core/precore mutations, which are considered positive events in the natural course of infection of 70–80% of chronically infected patients [71], can precede or follow the HBV DNA and ALT dynamics. Spontaneous HBeAg seroclearance followed by the recovery of HBV-specific T-cell functions, however, may result in hepatitis and liver disease [72], through T lymphocyte cytotoxic function [73], cytokine production, such as IL-6, IL-12 and TNF-α [74], and natural killer-induced INF-γ production [72].

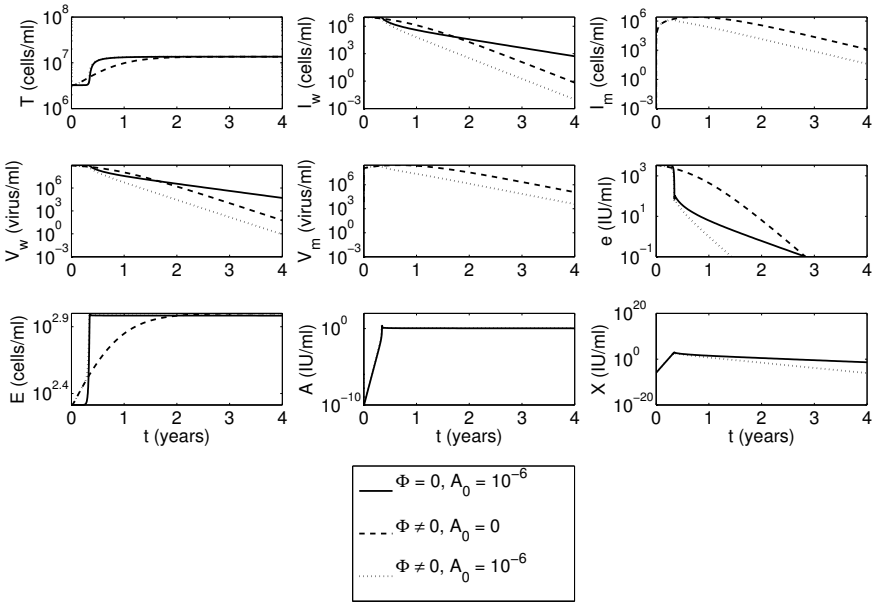

Figure 5. Dynamics of system (3.6) for $A_0 = 10^{-6}$ IU/mL and $\Phi = 0$ (solid curves); $A_0 = 0$ IU/mL and $\Phi = 0.12$ (dashed curves); $A_0 = 10^{-6}$ IU/mL and $\Phi = 0.12$ (dotted curves). Here, $s = 6$ mL/(IU×d), and all other parameters are given in Table 1.

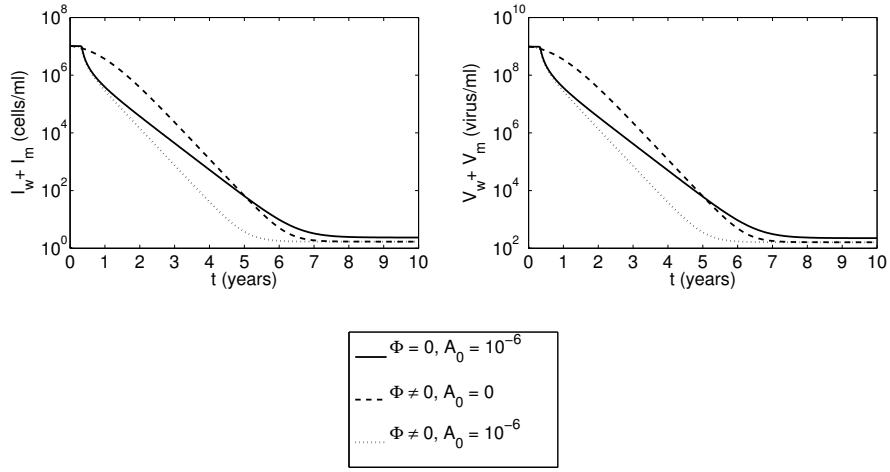

Figure 6. Dynamics of the total infected cell and virus populations, $I_w + I_m$ and $V_w + V_m$ for $A_0 = 10^{-6}$ IU/mL and $\Phi = 0$ (solid curves); $A_0 = 0$ IU/mL and $\Phi = 0.12$ (dashed curves); $A_0 = 10^{-6}$ IU/mL and $\Phi = 0.12$ (dotted curves). Here, $s = 6$ mL/(IU×d) , and all other parameters are given in Table 1.

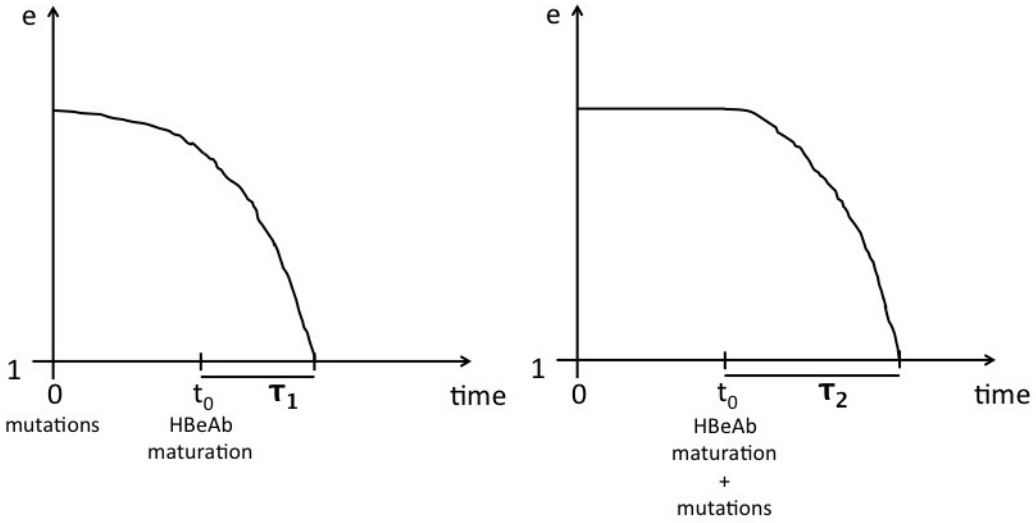

Figure 7. Cartoon of HBeAg seroclearance times $\tau_1(t_0, \Phi)$ (left) and $\tau_2(t_0, \Phi)$ (right).

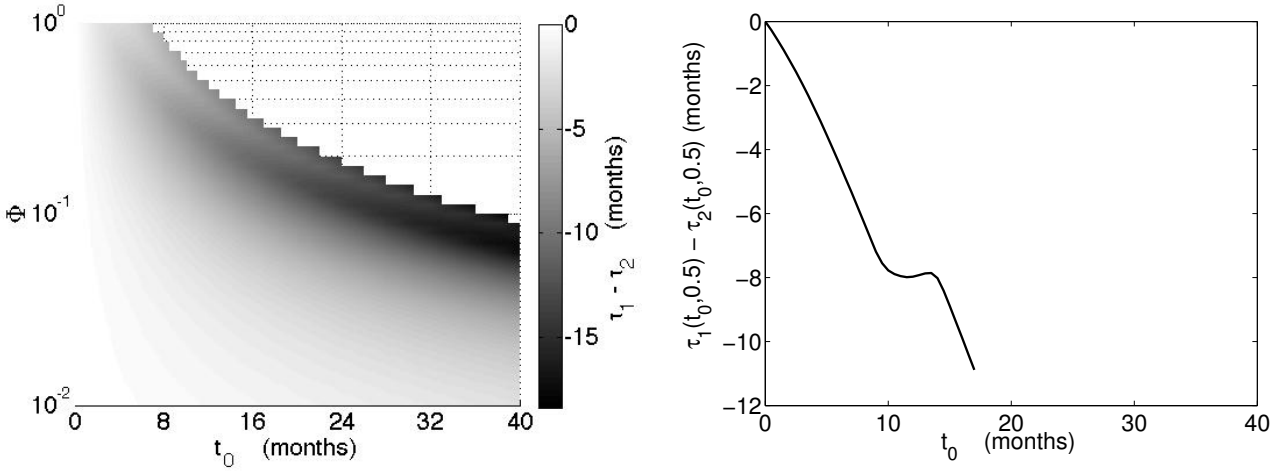

Figure 8. (Left) Heat map of $\tau_1(t_0, \Phi) - \tau_2(t_0, \Phi)$, the time between HBeAb formation and HBeAg seroclearance when mutations emerge at $t = 0$ and antibody emerges at time $t = t_0$, and when mutations and antibody emerge at $t = t_0$, versus time t_0 and fraction of core/precore mutations Φ. (Right) $\tau_1(t_0, \Phi) - \tau_2(t_0, \Phi)$ for fixed $\Phi = 0.5$. Parameters for wildtype and mutant populations are assumed to be equal and given in Table 1, $s = 6$ mL/(IU×d).

Since the order of sequential events leading to HBeAg loss is unknown (and patient dependent), we use model (3.6) to determine: (i) the amount of time it takes to reach HBeAg seroclearance following HBeAb expansion; (ii) the amount of monthly liver turnover, which is defined as the average liver loss due to immune response mediated killing each month [75] (here, the time period from HBeAb expansion to HBeAg seroclearance), for various fractions of core/precore mutations. For both questions core/precore mutations start at time $t = 0$ and HBeAb matures at time $t = t_0 \geq 0$.

As defined in the previous section, $\tau_1(t_0, \Phi)$ is the time between HBeAb expansion and HBeAg seroclearance (see Figure 7, left panel). We only consider ranges of t_0 and Φ where $\tau_1(t_0, \Phi)$ is positive, based on the assumption that HBeAb expansion happens before HBeAg seroclearance. Under these assumptions, we set

$$HL(t_0, \Phi) = \left(\int_{t_0}^{t_0+\tau_1(t_0,\Phi)} \left(\mu_w \frac{I_w(t)}{T_m} E(t) + \mu_m \frac{I_m(t)}{T_m} E(t) \right) dt \right) / \tau_1(t_0, \Phi), \tag{3.7}$$

to be the average monthly hepatocyte turnover over the $(t_0, t_0 + \tau_1(t_0, \Phi))$ time interval. Heat maps for $\tau_1(t_0, \Phi)$ and $HL(t_0, \Phi)$ are presented in Figure 9.

For large core/precore mutations, $\Phi > 0.5$, HBeAg seroclearance happens before antibody formation for large t_0 (see Figure 9, left panel, white region), and in the first 12 months post HBeAb expansion (t_0 + 12 months following the start of mutations) for small t_0 (see Figure 9, left panel, blue region). HBeAg loss is (almost) exclusively due to mutations. As Φ decreases, $\tau_1(t_0, \Phi)$ becomes less sensitive to the delay t_0 between the start of mutations and antibody expansion, indicating that antibodies gain more influence on the progression to HBeAg seroclearance. Finally, for small core/precore mutations, $\Phi < 0.01$, the time between HBeAb expansion and HBeAg seroclearance, $\tau_1(t_0, \Phi)$, is almost constant for a fixed Φ regardless of t_0 (in the range $0 \leq t_0 \leq 40$ months). This means that the initial HBeAg loss is almost exclusively antibody-driven and only the second phase decay is influenced by mutations. Previously, monthly hepatocyte turnover was estimated during acute HBV infections to range between $0.12 - 1$ T_m/month [32]. Our model predicts a monthly hepatocyte turnover of 0.4 T_m/month (see Figure 9, right panel, red region) for large Φ and small t_0 and 0.1 T_m/month for $\Phi < 0.01$, regardless of t_0 (in the range $0 \leq t_0 \leq 40$ months).

We next investigate how these results are altered in the presence of antiviral therapy.

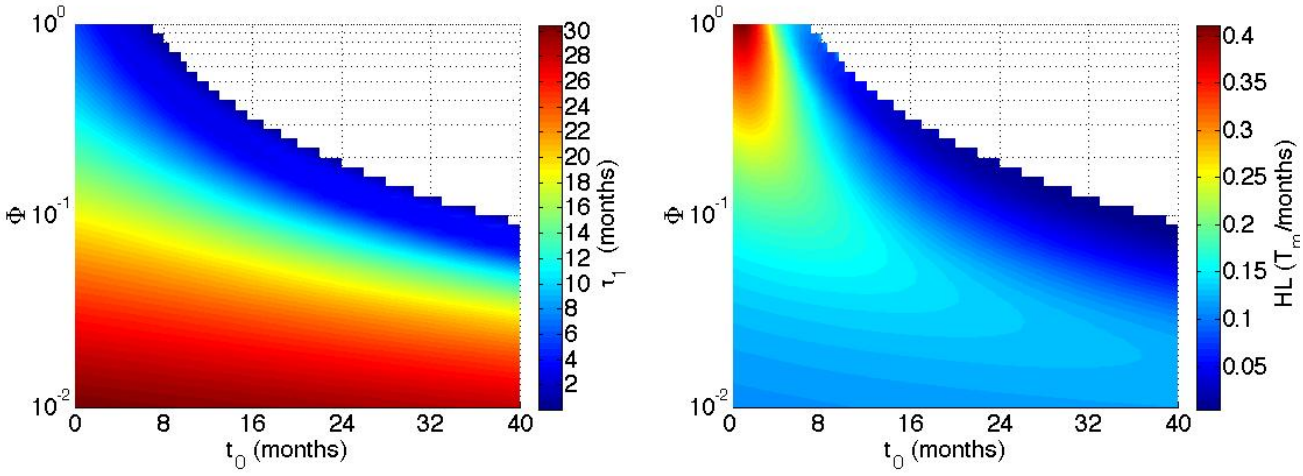

Figure 9. (Left) Heat map for $\tau_1(t_0, \Phi)$, the time between HBeAb expansion and HBeAg seroclearance, versus the time of HBeAb expansion t_0 and the fraction of core/precore mutations Φ. The corresponding parameters for wildtype and mutant populations are assumed to be equal and given in Table 1, and $s = 6$ mL/(IU×d). (Right) Heat map of $HL(t_0, \Phi)$, the average monthly hepatocyte loss between HBeAb expansion and HBeAg seroclearance due to CTLs killing, versus the time of HBeAb expansion t_0 and the fraction of core/precore mutations Φ. Mutations start at time 0.

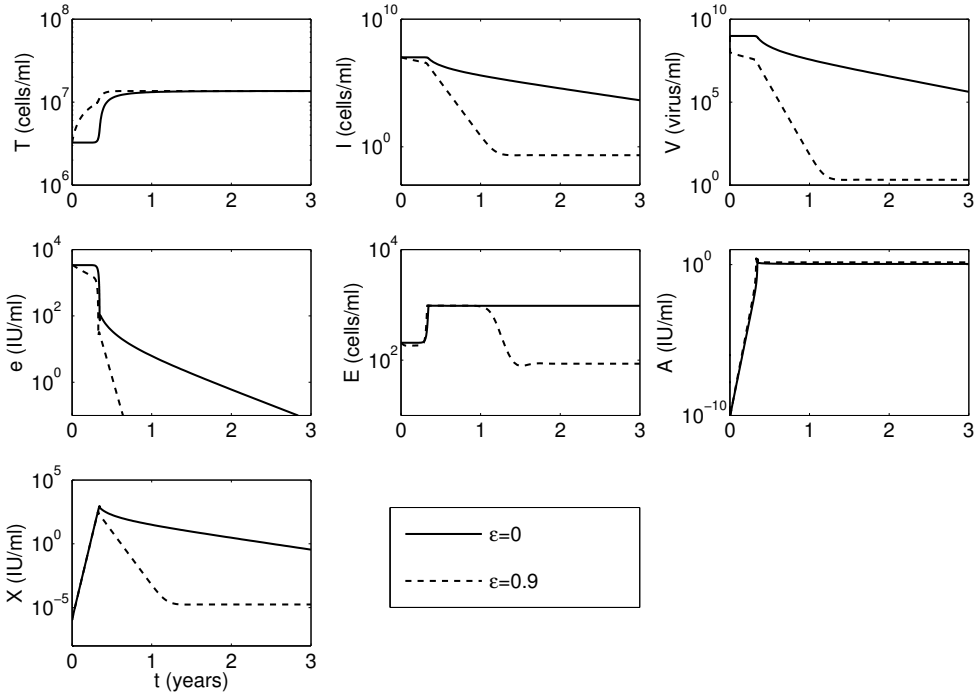

Figure 10. Dynamics of system (2.1) under treatment for $A_0 = 10^{-6}$ IU/mL, $s = 6$ mL/(IU×d), $\epsilon = 0$ (solid line), and $\epsilon = 0.9$ (dashed line). All other parameters are given in Table 1.

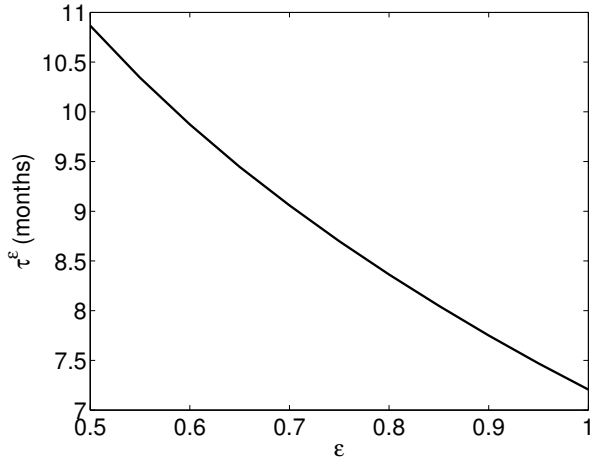

Figure 11. HBeAg seroclearance time τ^ϵ (in months past HBeAb expansion) versus treatment efficacy ϵ for $A_0 = 10^{-6}$ IU/mL, $s = 6$ mL/(IU×d), and all other parameters as in Table 1 (solid).

4. HBeAg dynamics during antiviral therapy

4.1. Treatment in the absence of mutations

We investigate how the dynamics presented in Figure 2 change when we consider the effects of nucleos(t)ide analogous antiviral treatment. Unless noted otherwise, we assume that treatment and HBeAb expansion occur concomitantly at time $t = 0$. NAs suppress viral replication [9,10]. We model this effect by reducing the virus production rate p by the treatment efficacy $0.5 < \epsilon < 1$. Hence, $p_{treat} = (1 - \epsilon)p$.

Under high treatment efficacy $\epsilon = 0.9$, virus undergoes a triphasic decay to a new equilibrium of 2 cp/mL: an instantaneous $0.94 \log_{10}$ drop in the first day, followed by a slower $0.5 \log_{10}$ decay over the next 4 months and finally a $6.4 \log_{10}$ decay over the next 9.6 months. The HBeAg does not decay during the first day, and follows a triphasic decay that reaches the limit of detection within 7.9 months following the start of therapy (see Figure 10, dashed curve). The HBeAg first phase decay is due to treatment induced virus loss, while the second and third decay phases present qualitative dynamics that are similar to the ones obtained in the absence of treatment: where HBeAb efficiently binds HBeAg, leading to the removal of the tolerogenic effect on the CTLs, which eventually control the HBeAg (infected cells) loss (see Figure 10, dashed vs. solid curves). During the third phase, the decay rates of virus and HBeAg levels are steeper during treatment due to CTL-mediated removal of lower virus (infected cell) populations. Treatment efficacies (in the range considered, $0.5 < \epsilon < 1$) influence the time of HBeAg seroclearance, with fast HBeAg seroclearance for high ϵ (see Figure 11). In the absence of treatment, HBeAg has a seroclearance time of 2.83 years. By contrast, HBeAg seroclearance time decreases to 11.8 and 7.2 months for $\epsilon = 0.5$ and $\epsilon = 0.99$ (see Figure 11).

4.2. Treatment in the presence of mutations

We next examine how treatment with various drug efficacies ϵ influences: (i) the amount of time it takes to reach HBeAg seroclearance after HBeAb expansion; and (ii) the monthly amount of liver turnover between HBeAb expansion and HBeAg seroclearance HL, under various fractions of core/precore mutations (see Figure 12). For both questions we assume that mutations start at time $t = 0$, and treatment and HBeAb expansion occur concomitantly at time $t = t_0 \in [0, 40]$ months. As before, we define $\tau_1(t_0, \Phi)$ to be the time between HBeAb expansion and HBeAg seroclearance.

As in the absence of treatment, for large $\Phi > 0.5$ and large t_0, HBeAg seroclearance happens before antibody formation for all ϵ (see Figure 12, for $\epsilon = 0.7$). HBeAg loss is exclusively due to mutations. As Φ decreases, $\tau_1(t_0, \Phi)$ becomes less sensitive to the delay t_0 between the start of mutations and antibody expansion, indicating that antibodies gain more influence on the progression to HBeAg seroclearance. Finally, for small core/precore mutations, $\Phi < 0.01$, the time between HBeAb expansion and HBeAg seroclearance, $\tau_1(t_0, \Phi)$, is almost constant regardless of t_0 (in the range $0 \leq t_0 \leq 40$ months). This means that the initial HBeAg loss is almost exclusively antibody-driven and only the second phase decay is influenced by mutations. After HBeAb expansion, HBeAg is cleared faster under treatment with $\epsilon = 0.7$ than in the absence of treatment (compare Figures 12 and 9, left panels). Furthermore, our model predicts that for $\epsilon = 0.7$ the monthly hepatocyte turnover is greatest for large Φ and small t_0, up to 0.18 T_m/month (see 12, right panel, red region), lower than the 0.4 T_m/month in the absence of treatment. As Φ decreases, and $\tau_1(t_0, \Phi)$ increases, the monthly

hepatocyte turnover decreases to 0.12 T_m/month for $\Phi < 0.01$ regardless of t_0 (in the range $0 \leq t_0 \leq 40$ months), higher than the 0.1 T_m/month observed in the absence of treatment. We find that low drug efficacy yields an increase in monthly hepatocyte turnover for $\Phi < 0.01$. For example, for $\epsilon = 0.5$, the monthly hepatocyte turnover is 0.16 T_m/month, while for $\epsilon = 0.99$, the average monthly hepatocyte turnover is 0.1 T_m/month, *i.e.* equal to the average monthly hepatocyte turnover in the absence of treatment. However, since HBeAg seroclearance is faster under treatment, the total hepatocyte turnover is significantly reduced.

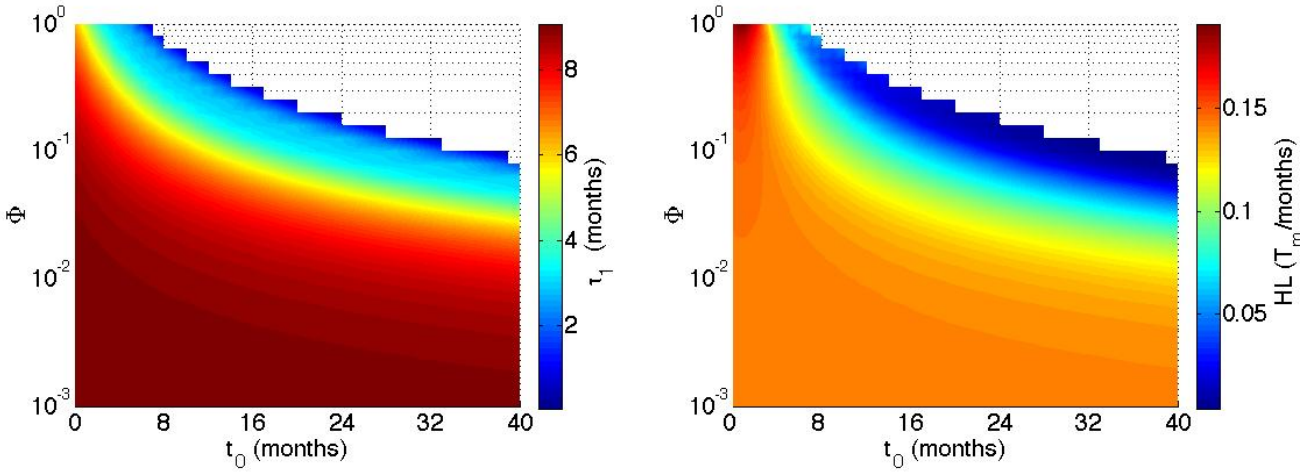

Figure 12. (Left) Heat map for $\tau_1(t_0, \Phi)$, the time between HBeAb expansion and HBeAg seroclearance, versus the time of HBeAb expansion t_0 and the fraction of core/precore mutations Φ. The corresponding parameters for wildtype and mutant populations are assumed to be equal and given in Table 1, and $s = 6$ mL/(IU×d). (Right) Heat map of $HL(t_0, \Phi)$, the average monthly hepatocyte loss between HBeAb expansion and HBeAg seroclearance due to CTLs killing, versus the time of HBeAb expansion t_0 and the fraction of core/precore mutations Φ, for $\epsilon = 0.7$. Mutations start at time 0.

5. Discussion and conclusion

We developed a mathematical model describing the host-pathogen interactions during HBeAg-positive chronic hepatitis B virus infections, with a focus on the effects of HBeAb expansion on disease progression and in particular HBeAg seroclearance. HBeAg, a secretory protein described as an immune tolerogen which downregulates the cellular immune responses [6], is removed when HBeAb is produced. The moment at which HBeAb production starts, its mechanistic interactions with HBeAg and other immune responses, or the timing of HBeAg seroclearance are not well understood. We employed a mathematical modeling approach to provide insight into antibody formation and HBeAg seroclearance. Previous mathematical models have investigated the interplay between hepatocytes, infected hepatocytes, HBV virus [30], CTL-mediated immune responses [31, 34, 45–47], humoral-mediated immune responses [48, 49], a class of subviral particles [49], and HBeAg [50]. To our knowledge, however, only one paper, in the context of occult HBV infection, has incorporated the dynamics of HBeAb [44].

We used the model to determine the interplay between HBeAb and CTL immune responses on HBeAg seroclearance in the absence and presence of treatment. Our model predicted that, in the absence of treatment, a combination of CTL and antibody responses are needed to achieve HBeAg seroclearance and viral remission. We found that HBeAg seroclearance follows several key stages: (1) newly matured HBeAb expand, bind HBeAg to form HBeAg-HBeAb immune complexes, which are removed via phagocytosis; (2) HBeAg population decays to levels that no longer affect CTLs activity, leading to CTLs activation and expansion; (3) infected cells are killed by CTLs; and, consequently, (4) less HBeAgs are produced and eventually decay below 0.1 IU/mL (called seroclearance level). We investigated the relationship between HBeAg seroclearance and the rate of HBeAb production and found that bigger HBeAb production rates lead to shorter times to HBeAg seroclearance.

Host-virus predictors for HBeAg seroclearance are limited. Mutations of HBV in its core or precore region result in loss of expression of HBeAg by hepatocytes infected with the mutated virus [66, 67]. We assumed that these mutations are followed by antibody formation and eventual HBeAg seroclearance, and investigated how core/precore mutations influence the time between HBeAb expansion and HBeAg seroclearance and the hepatocyte turnover. We found that large fractions of mutations result in fast HBeAg seroclearance without the help of HBeAbs and high monthly hepatocyte turnover. Intermediate fractions of mutations result in longer seroclearance times and lower monthly hepatocyte turnover. For small fractions of mutations HBeAg seroclearance is driven almost exclusively by HBeAbs, the seroclearance times are longest and monthly hepatocyte turnover is lowest. Furthermore, we found that mutations can clear HBeAg even in the absence of antibodies.

Increased HBeAg seroconversion rates after one year of NA treatment, regardless of NAs efficacy, have been observed in clinical studies [26]. We predicted that, regardless of the treatment efficacy, the time from HBeAb expansion to HBeAg seroclearance is significantly shortened by treatment, ranging between 7 month for high efficacy treatment and 11 months for low efficacy treatment, *i.e.* within one year, compared to 2.8 years in the absence of treatment. Our model does not, however, inform why a prolonged duration (several years) of high efficacy treatment is deleterious to the achievement of HBeAg seroconversion [28].

Under treatment, as in the absence of treatment, mutations influence the length of time between HBeAb expansion and HBeAg seroclearance as well as the amount of monthly hepatocyte turnover. The qualitative results are the same as in the untreated case, with fastest HBeAg seroclearance and highest monthly hepatocyte turnover for large fractions and slowest HBeAg seroclearance and lowest monthly hepatocyte turnover for small fractions of mutations. While the time to HBeAg seroclearance under treatment is always shorter than in the absence of treatment, the monthly hepatocyte turnover is decreased only for large fractions. Small fractions of mutations yield an increased monthly hepatocyte turnover under treatment.

When we modeled core/precore mutations, we assumed similar characteristics for the wildtype and mutant virus strains and their corresponding infected cell classes. Studies have reported different half-lives for the wildtype and mutant virus strains, although the exact values vary. Dandri *et al.* reported average half-lives of 46 and 2.5 minutes [76]. Ribeiro *et al.* reported half-lives of 25.2 and 13.1 hours and shorter half-lives of cells infected by mutant compared to wildtype virus, 12.1 days versus 16 days [77]. Lastly, it has been suggested that cells that express mutant virus can lose the ability to express wildtype virus [78]. This can be modeled by assuming that a fraction z of cells infected with

the wildtype virus transitions into the population of cells infected with the mutant virus. We have investigated how differences in the two strains affect our results by considering a 10-fold increase in the mutant clearance rate, combined with a 1.3-fold increase in the clearance rate of cells infected with the mutant virus, and a $z = 0.01$ transitioning rate from wildtype to mutant infection. We found changes in the timing of HBeAg seroclearance, with the longest time occurring when mutant clearance rates are increased and the transition is zero, and the shortest time occurring when the mutant clearance rates are kept at the wild-type levels and the transition is non-negative (see Appendix 3, heterogeneity in infected and virus populations section, Figures S15 and S16).

Our model assumes that more than 75% of the liver is infected during chronic HBV infections. While such large values have been reported in acute infections [31, 79], it is possible that fewer hepatocytes get infected during chronic disease [80]. We performed a sensitivity analysis on the infectivity parameter β which showed that our results are sensitive to changes in β, and, consequently, to having a lower amount of the liver infection in the first 2 years (Appendix 3, sensitivity analysis section, Figure S4). Further work is needed to determine how the results will change if we assume lower level of liver infection. There are many other parameters for which we have limited quantitative information. Most of these parameters were kept fixed in our model. The model's sensitivities to a number of these parameters are shown in Figures S2 – S11 (Appendix 3, sensitivity analysis section). Another limitation of our model is that the production rate of virus is unaffected by the non-cytolytic effects of the effector cell population. Effector cells produce cytokines such as IFN-γ that inhibit the HBV replication and thus, the HBV virions production rate. Further work is needed to determine how the results will change if we assume that effector cells inhibit the virus production.

In conclusion, we have built a mathematical model of HBeAg seroclearance and investigated how HBeAb and CTL work together to secure the transition into an HBeAg-negative HBV infection and how the efficacy of drug therapy affects the timing to HBeAg seroclearance. Such results are important for understanding this milestone event in HBV natural history and can be used to inform human interventions.

Acknowledgments

SMC and SK acknowledge funding from National Science Foundation grant No. 1813011. We thank the reviewers for the valuable comments and suggestions.

Conflict of interest

The authors declare there is no conflict of interest.

References

1. J. Hou, Z. Liu and F. Gu, Epidemiology and prevention of hepatitis B virus infection, *Int. J. Med. Sci.*, **2** (2005), 50.
2. European Association for the study of the Liver, EASL 2017 clinical practice guidelines on the management of hepatitis B virus infection, *J. Hepatol.*, **67** (2017), 370–398.

3. J. E. Bennett, R. Dolin and M. J. Blaser, *Mandell, Douglas and Bennett's Principles and Practice of Infectious Disease*, 8th edition, Elsevier Saunders, Philadelphia, 2015.
4. G. Fattovich, F. Bortolotti and F. Donato, Natural history of chronic hepatitis B: Special emphasis on disease progression and prognostic factors, *J. Hepatol.*, **48** (2008), 335–352.
5. D. Milich and T. J. Liang, Exploring the biological basis of hepatitis B e antigen in hepatitis B virus infection, *Hepatology*, **38** (2003), 1075–1086.
6. Y. Han, J. Li, L. Jiang, et al., Regulation of B7-H1 expression on peripheral monocytes and IFN-γ secretion in T lymphocytes by HBeAg, *Cell. Immunol.*, **283** (2013), 25–30.
7. W. R. Kim, S. L. Flamm, A. M. Di Bisceglie, et al., Serum activity of alanine aminotransferase (ALT) as an indicator of health and disease, *Hepatology*, **47** (2008), 1363–1370.
8. R. Marug'an and S. Garz'on, DNA-guided hepatitis B treatment, viral load is essential, but not sufficient, *World J. Gastroenterol.*, **15** (2009), 423–430.
9. V. Rijckborst and H. L. Janssen, The role of interferon in hepatitis B therapy, *Curr. Hepat. Rep.*, **9** (2010), 231–238.
10. J. Fung, C.-L. Lai, W.-K. Seto, et al., Nucleoside/nucleotide analogues in the treatment of chronic hepatitis B, *J. Antimicrob. Chemother.*, **66** (2011), 2715–2725.
11. European Association for the study of the Liver, EASL clinical practice guidelines: management of chronic hepatitis b virus infection, *J. Hepatol.*, **57** (2012), 167–185.
12. W. Zhang, D. Zhang, X. Dou, et al., Consensus on pegylated interferon alpha in treatment of chronic hepatitis B, *J. Clin. Transl. Hepatol.*, **6** (2018), 1.
13. G. Papatheodoridis, I. Vlachogiannakos, E. Cholongitas, et al., Discontinuation of oral antivirals in chronic hepatitis B: A systematic review, *Hepatology*, **63** (2016), 1481–1492.
14. A. S. J. Woo, R. Kwok and T. Ahmed, Alpha-interferon treatment in hepatitis B, *Ann. Transl. Med.*, **5** (2017), 159.
15. S. J. Hadziyannis, Update on hepatitis B virus infection: focus on treatment, *J. Clin. Transl. Hepatol.*, **2** (2014), 285.
16. J. Vlachogiannakos and G. V. Papatheodoridis, Hepatitis B: Who and when to treat?, *Liver Int.*, **38** (2018), 71–78.
17. Y.-F. Liaw, HBeAg seroconversion as an important end point in the treatment of chronic hepatitis B, *Hepatol. Int.*, **3** (2009), 425–433.
18. C.-K. Hui, N. Leung, T. W. Shek, et al., Sustained disease remission after spontaneous HBeAg seroconversion is associated with reduction in fibrosis progression in chronic hepatitis B chinese patients, *Hepatology*, **46** (2007), 690–698.
19. H.-I. Yang, S.-N. Lu, Y.-F. Liaw, et al., Hepatitis B e antigen and the risk of hepatocellular carcinoma, *N. Engl. J. Med.*, **347** (2002), 168–174.
20. Y.-S. Hsu, R.-N. Chien, C.-T. Yeh, et al., Long-term outcome after spontaneous HBeAg seroconversion in patients with chronic hepatitis B, *Hepatology*, **35** (2002), 1522–1527.

21. C.-M. Chu, S.-J. Hung, J. Lin, et al., Natural history of hepatitis be antigen to antibody seroconversion in patients with normal serum aminotransferase levels, *Am. J. Med.*, **116** (2004), 829–834.
22. S.-M. Lin, M.-L. Yu, C.-M. Lee, et al., Interferon therapy in HBeAg positive chronic hepatitis reduces progression to cirrhosis and hepatocellular carcinoma, *J. Hepatol.*, **46** (2007), 45–52.
23. C.-M. Chu and Y.-F. Liaw, Spontaneous relapse of hepatitis in inactive HBsAg carriers, *Hepatol. Int.*, **1** (2007), 311–315.
24. C.-M. Chu and Y.-F. Liaw, Chronic hepatitis B virus infection acquired in childhood: special emphasis on prognostic and therapeutic implication of delayed HBeAg seroconversion, *J. Viral Hepat.*, **14** (2007), 147–152.
25. C.-M. Chu and Y.-F. Liaw, Predictive factors for reactivation of hepatitis B following hepatitis B e antigen seroconversion in chronic hepatitis B, *Gastroenterology*, **133** (2007), 1458–1465.
26. H. Dakin, C. Fidler and C. Harper, Mixed treatment comparison meta-analysis evaluating the relative efficacy of nucleos(t)ides for treatment of nucleos(t)ide-naive patients with chronic hepatitis B, *Value Health*, **13** (2010), 934–945.
27. A. Wiens, L. Lenzi, R. Venson, et al., Comparative efficacy of oral nucleoside or nucleotide analog monotherapy used in chronic hepatitis B: a mixed-treatment comparison meta-analysis, *Pharmacotherapy*, **33** (2013), 144–151.
28. T. Xing, H. Xu, L. Cao, et al., HBeAg seroconversion in HBeAg-positive chronic hepatitis B patients receiving long-term nucleos(t)ide analog treatment: a systematic review and network meta-analysis, *PLoS One*, **12** (2017), e0169444.
29. M. Yuen, H. Yuan, C. Hui, et al., A large population study of spontaneous HBeAg seroconversion and acute exacerbation of chronic hepatitis B infection: implications for antiviral therapy, *Gut*, **52** (2003), 416–419.
30. M. Nowak, S. Bonhoeffer, A. Hill, et al., Viral dynamics in hepatitis B virus infection, *Proc. Natl. Acad. Sci. U.S.A.*, **93** (1996), 4398–4402.
31. S. Ciupe, R. Ribeiro, P. Nelson, et al., The role of cells refractory to productive infection in acute hepatitis B viral dynamics, *Proc. Natl. Acad. Sci. U.S.A.*, **104** (2007), 5050–5055.
32. A. Goyal, R. M. Ribeiro and A. S. Perelson, The role of infected cell proliferation in the clearance of acute HBV infection in humans, *Viruses*, **9** (2017), 350.
33. A. Neumann, N. Lam, H. Dahari, et al., Hepatitis C viral dynamics in vivo and the antiviral efficacy of interferon-α therapy, *Science*, **282** (1998), 103–107.
34. Y. Ji, W. Li, L. Min, et al., A mathematical model for anti-HBV infection treatment with lamivudine and curative effect prediction, in *Control and Automation, 2007. ICCA 2007. IEEE International Conference on*, IEEE, 2007, 2485–2488.
35. S. Gourley, Y. Kuang and J. Nagy, Dynamics of a delay differential model of hepatitis B virus, *J. Biol. Dyn.*, **2** (2008), 140–153.
36. S. Eikenberry, S. Hews, J. Nagy, et al., The dynamics of a delay model of HBV infection with logistic hepatocyte growth, *Math. Biosci. Eng.*, **6** (2009), 283–299.

37. H. Dahari, E. Shudo, R. M. Ribeiro, et al., Modeling complex decay profiles of hepatitis B virus during antiviral therapy, *Hepatology*, **49** (2009), 32–38.

38. S. R. Lewin, R. M. Ribeiro, T. Walters, et al., Analysis of hepatitis B viral load decline under potent therapy: complex decay profiles observed, *Hepatology*, **34** (2001), 1012–1020.

39. A. U. Neumann, S. Phillips, I. Levine, et al., Novel mechanism of antibodies to hepatitis B virus in blocking viral particle release from cells, *Hepatology*, **52** (2010), 875–885.

40. J. Forde, S. Ciupe, A. Cintron-Arias, et al., Optimal control of drug therapy in a hepatitis B model, *Appl. Sci*, **6** (2016), 219.

41. A. Carracedo Rodriguez, M. Chung and S. Ciupe, Understanding the complex patterns observed during hepatitis B virus therapy, *Viruses*, **9** (2017), 117.

42. A. Goyal and J. M. Murray, Modelling the impact of cell-to-cell transmission in hepatitis B virus, *PLoS One*, **11** (2016), e0161978.

43. J. M. Murray and A. Goyal, In silico single cell dynamics of hepatitis B virus infection and clearance, *J. Theor. Biol.*, **366** (2015), 91–102.

44. A. Goyal and R. Chauhan, The dynamics of integration, viral suppression and cell-cell transmission in the development of occult hepatitis B virus infection, *J. Theor. Biol.*, **455** (2018), 269–280.

45. S. Ciupe, R. Ribeiro, P. Nelson, et al., Modeling the mechanisms of acute hepatitis B virus infection, *J. Theor. Biol.*, **247** (2007), 23–35.

46. C. Long, H. Qi and S. Huang, Mathematical modeling of cytotoxic lymphocyte-mediated immune response to hepatitis B virus infection, *J. Biomed. Biotechnol.*, **2008** (2008), 743690.

47. H. Kim, H. Kwon, T. Jang, et al., Mathematical modeling of triphasic viral dynamics in patients with HBeAg-positive chronic hepatitis B showing response to 24-week clevudine therapy, *PLoS One*, **7** (2012), e50377.

48. N. Yousfi, K. Hattaf and A. Tridane, Modeling the adaptive immune response in HBV infection, *J. Math. Biol.*, **63** (2011), 933–957.

49. S. Ciupe, R. Ribeiro and A. Perelson, Antibody response during hepatitis B viral infection, *PLoS Comput. Biol.*, **10** (2014), e1003730.

50. S. Ciupe and S. Hews, Mathematical models of e-antigen mediated immune tolerance and activation following prenatal HBV infection, *PLoS One*, **7** (2012), e39591.

51. J. Rozga, Hepatocyte proliferation in health and in liver failure, *Med. Sci. Monit.*, **8** (2002), RA32–RA38.

52. L. Allweiss and M. Dandri, The role of cccDNA in HBV maintenance, *Viruses*, **9** (2017), 156.

53. D. R. Milich, M. K. Chen, J. L. Hughes, et al., The secreted hepatitis B precore antigen can modulate the immune response to the nucleocapsid: a mechanism for persistence, *J. Immunol.*, **160** (1998), 2013–2021.

54. M. Oprea and A. S. Perelson, Exploring the mechanisms of primary antibody responses to t cell-dependent antigens, *J. Theor. Biol.*, **181** (1996), 215–235.

55. J. S. Dooley, A. Lok, A. K. Burroughs, et al., *Sherlock's diseases of the liver and biliary system*, John Wiley & Sons, 2011.

56. A.-K. Sohlenius-Sternbeck, Determination of the hepatocellularity number for human, dog, rabbit, rat and mouse livers from protein concentration measurements, *Toxicol. In Vitro*, **20** (2006), 1582–1586.

57. J. Murray, R. Purcell and S. Wieland, The half-life of hepatitis B virions, *Hepatology*, **44** (2006), 1117–1121.

58. S. A. Whalley, J. M. Murray, D. Brown, et al., Kinetics of acute hepatitis B virus infection in humans, *J. Exp. Med.*, **193** (2001), 847–854.

59. R. Ahmed and D. Gray, Immunological memory and protective immunity: understanding their relation, *Science*, **272** (1996), 54–60.

60. S. E. Brown, C. R. Howard, A. J. Zuckerman, et al., Determination of the affinity of antibodies to hepatitis B surface antigen in human sera, *J. Immunol. Methods*, **72** (1984), 41–48.

61. S. Stein, J. Ware and R. Woods, Serum immunoglobulins: Methods for the determination of normal values in international units, *J. Immunol. Methods*, **16** (1977), 371–384.

62. T. Igarashi, C. Brown, A. Azadegan, et al., Human immunodeficiency virus type 1 neutralizing antibodies accelerate clearance of cell–free virions from blood plasma, *Nat. Med.*, **5** (1999), 211.

63. G. D. Tomaras, N. L. Yates, P. Liu, et al., Initial B-cell responses to transmitted human immunodeficiency virus type 1: Virion-binding immunoglobulin M (IgM) and IgG antibodies followed by plasma Anti-gp41 antibodies with ineffective control of initial viremia, *J. Virol.*, **82** (2008), 12449–12463,

64. P. T. Kennedy, E. Sandalova, J. Jo, et al., Preserved T-cell function in children and young adults with immune-tolerant chronic hepatitis B, *Gastroenterology*, **143** (2012), 637–645.

65. S. Cai, Z. Li, T. Yu, et al., Serum hepatitis B core antibody levels predict HBeAg seroconversion in chronic hepatitis B patients with high viral load treated with nucleos(t)ide analogs, *Infect. Drug Resist.*, **11** (2018), 469.

66. H. Okamoto, F. Tsuda, Y. Akahane, et al., Hepatitis B virus with mutations in the core promoter for an e antigen-negative phenotype in carriers with antibody to e antigen, *J. Virol.*, **68** (1994), 8102–8110.

67. W. Carman, S. Hadziyannis, M. McGarvey, et al., Mutation preventing formation of hepatitis B e antigen in patients with chronic hepatitis B infection, *Lancet*, **334** (1989), 588–591.

68. S. F. Baqai, J. Proudfoot, H. Y. Debbie, et al., High rate of core promoter and precore mutations in patients with chronic hepatitis B, *Hepatol. Int.*, **9** (2015), 209–217.

69. N. Kamijo, A. Matsumoto, T. Umemura, et al., Mutations of pre-core and basal core promoter before and after hepatitis B e antigen seroconversion, *World J. Gastroenterol.*, **21** (2015), 541.

70. H. Okamoto, S. Yotsumoto, Y. Akahane, et al., Hepatitis B viruses with precore region defects prevail in persistently infected hosts along with seroconversion to the antibody against e antigen., *J. Virol.*, **64** (1990), 1298–1303.

71. J.-H. Kao, P.-J. Chen and D.-S. Chen, Recent advances in the research of hepatitis B virus-related hepatocellular carcinoma: epidemiologic and molecular biological aspects, *Adv. Cancer Res.*, **108** (2010), 21–72.

72. E.-C. Shin, P. S. Sung and S.-H. Park, Immune responses and immunopathology in acute and chronic viral hepatitis, *Nat. Rev. Immunol.*, **16** (2016), 509–523.

73. C. Ferrari, HBV and the immune response, *Liver Int.*, **35** (2015), 121–128.

74. D. He, G. Yan and Y. Wang, Serum levels of interleukin-12 in various clinical states with hepatitis B virus infection, *Cell. Immunol.*, **272** (2012), 162–165.

75. S. M. Ciupe, Modeling the dynamics of hepatitis B infection, immunity, and drug therapy, *Immunol. Rev.*, **285** (2018), 38–54.

76. M. Dandri, J. M. Murray, M. Lutgehetmann, et al., Virion half-life in chronic hepatitis B infection is strongly correlated with levels of viremia, *Hepatology*, **48** (2008), 1079–1086.

77. R. M. Ribeiro, G. Germanidis, K. A. Powers, et al., Hepatitis B virus kinetics under antiviral therapy sheds light on differences in hepatitis B e antigen positive and negative infections, *J. Infect. Dis.*, **202** (2010), 1309–1318.

78. W. Mason, S. Litwin, C. Xu, et al., Hepatocyte turnover in transient and chronic hepadnavirus infections, *J. Viral Hepat.*, **14** (2007), 22–28.

79. L. G. Guidotti, R. Rochford, J. Chung, et al., Viral clearance without destruction of infected cells during acute hbv infection, *Science*, **284** (1999), 825–829.

80. E. Rodríguez-Iñigo, L. Mariscal, J. Bartolomé, et al., Distribution of hepatitis B virus in the liver of chronic hepatitis C patients with occult hepatitis B virus infection, *J. Med. Virol.*, **70** (2003), 571–580.

Supplementary

Appendix 1. Stability analysis of the system without HBeAb. System (3.2) has the following non-negative equilibria: no liver, no CTL responses

$$S_1^{noA} = (0, 0, 0, 0, 0), \tag{5.1}$$

infection free state

$$S_2^{noA} = (T_m, 0, 0, 0, 0), \tag{5.2}$$

no liver under CTL responses

$$S_3^{noA} = \left(0, 0, 0, 0, \frac{E_m(s_E - d_E)}{s_E}\right), \tag{5.3}$$

clearance due to CTLs

$$S_4^{noA} = \left(T_m, 0, 0, 0, \frac{E_m(s_E - d_E)}{s_E}\right), \tag{5.4}$$

infection in the absence of CTL responses

$$S_5^{noA} = \left(0, T_m, \frac{T_m p}{c}, \frac{T_m \pi}{\delta_e}, 0\right) \tag{5.5}$$

and infection under immune anergy. There are up to four solutions of this form

$$S_6^{noA} = \left(\bar{T}(\bar{I}), \bar{I}, \frac{p}{c}\bar{I}, \frac{\pi}{\delta_e}\bar{I}, \bar{E}(\bar{I})\right), \tag{5.6}$$

where

$$\bar{T}(\bar{I}) = \frac{((\alpha\delta_e - \pi\sigma d_E)\bar{I} + \delta_e(s_E - d_E))E_m c\mu}{\delta_e\beta p(\alpha\bar{I} + s_E)},$$

$$\bar{E}(\bar{I}) = \frac{((\alpha\delta_e - \pi\sigma d_E)\bar{I} + \delta_e(s_E - d_E))E_m}{\delta_e(\alpha\bar{I} + s_E)},$$

and $\bar{I}$ is a root of the fourth degree polynomial

$$C_4\bar{I}^4 + C_3\bar{I}^3 + C_2\bar{I}^2 + C_1\bar{I} + C_0,$$

with

$$C_4 = \alpha^2\delta_e^2\beta^2p^2r,$$

$$C_3 = 2\left(\left(\frac{(T_m(E_m\mu - r)\alpha + 2rs_E)\beta p}{2} + cE_m\alpha r\mu\right)\delta_e - \pi\sigma E_m\left(\frac{\beta T_m p}{2} + cr\right)\mu d_E\right)\delta_e p\alpha\beta,$$

$$C_2 = \left(c^2E_m^2\alpha^2r\mu^2 - p\mu\left(-2T_m\left(s_E - \frac{d_E}{2}\right)\beta p + cr(T_m\alpha + 2d_E - 4s_E)\right)\alpha\beta E_m - 2s_E\left(T_m\alpha - \frac{s_E}{2}\right)rp^2\beta^2\right)\delta_e^2$$
$$- 2\pi\sigma E_m\left(c^2E_m\alpha r\mu - \frac{(-\beta T_m p s_E + cr(T_m\alpha - 2s_E))p\beta}{2}\right)\mu d_E\delta_e + E_m^2c^2d_E^2\mu^2\pi^2r\sigma^2,$$

$$C_1 = 2\delta_2\left(c^2r\mu^2(s_E - d_E)(-d_E\pi\sigma + \alpha\delta_e)E_m^2\right.$$
$$- p\mu\left(\left(\left(-s_E^2 + (T_m\alpha d_E)s_E - \frac{\alpha T_m d_E}{2}\right)cr - \frac{\beta T_m p s_E(s_E - d_E)}{2}\right)\delta_e - \frac{c\sigma r T_m\pi s_E d_E}{2}\right)kE_m$$
$$\left. - \frac{\delta_e\beta^2rT_mp^2s_E^2}{2}\right),$$

$$C_0 = (c\mu(s_E - d_E)E_m - \beta T_m p s_E)r\delta_e^2c(s_E - d_E)\mu E_m.$$

Equilibria S_1^{noA} and S_3^{noA} are solutions in which the total hepatocyte population is zero, corresponding to the death of the patient.

Theorem 5.1. *Equilibria S_1^{noA} and S_3^{noA} are unstable.*

Proof. The Jacobian of system (3.2) evaluated at S_1^{noA} or S_3^{noA} has eigenvalue $\lambda_1 = r > 0$. Hence S_1^{noA} and S_3^{noA} are unstable equilibria. □

Equilibria S_2^{noA} and S_4^{noA} are solutions in which the infection is cleared. In S_4^{noA} a population of memory cells persists over time, while in S_2^{noA} CTLs go extinct.

Theorem 5.2. *Equilibrium S_2^{noA} is unstable.*

Proof. Using *Maple* we find that the Jacobian of system (3.2) evaluated at S_2^{noA} has the eigenvalue

$$\lambda_1 = -\frac{c}{2} + \frac{\sqrt{4T_m\beta p + c^2}}{2},$$

which is always positive. Hence S_2^{noA} is an unstable equilibrium. □

Theorem 5.3. *Equilibrium S_4^{noA} exists and is locally asymptotically stable iff $s_E > d_E$ and $\frac{T_m\beta p s_E}{E_m c\mu(s_E - d_E)} < 1$.*

Proof. Using *Maple* we find that the Jacobian of system (3.2) evaluated at S_4^{noA} has two eigenvalues $\lambda_1 = -r$ and $\lambda_2 = -\delta_e$ which are always negative. A third eigenvalue $\lambda_3 = d_E - s_E$ is negative iff $s_E > d_E$. The remaining two eigenvalues are

$$\lambda_{4,5} = \frac{1}{2s_E}\left(-(cs_E + E_m\mu(s_e - d_E)) \pm \sqrt{(cs_E + E_m\mu(s_e - d_E))^2 + 4s_E(T_m\beta p s_E - E_m c\mu(s_E - d_E))}\right).$$

If $s_E > d_E$, then $(cs_E + E_m\mu(s_e - d_E)) > 0$ and hence $Re(\lambda_5) < 0$. For λ_4 we find

$$Re(\lambda_4) < 0 \Longleftrightarrow \frac{T_m\beta p s_E + E_m c d_E\mu}{E_m c\mu s_E} < 1 \Longleftrightarrow \frac{T_m\beta p s_E}{E_m c\mu(s_E - d_E)} < 1.$$

□

In equilibria S_5^{noA} and S_6^{noA} virus is not cleared. S_5^{noA} represents a state in which CTLs have vanished and the entire liver is infected, while S_6^{noA} is a state in which CTLs are ineffective.

Theorem 5.4. *Equilibrium S_5^{noA} is locally asymptotically stable iff $\frac{\delta_e(T_m\alpha + s_E)}{d_E(T_m\pi\sigma + \delta_e)} < 1$.*

Proof. Using *Maple* we find that the Jacobian of system (3.2) evaluated at S_5^{noA} has four eigenvalues $\lambda_1 = -r$, $\lambda_2 = -\delta_e$, $\lambda_3 = -c$, and $\lambda_4 = -\frac{T_m\beta p}{c}$ which are always negative. The fifth eigenvalue

$$\lambda_5 = \frac{\delta_e(T_m\alpha + s_E) - d_E(T_m\pi\sigma + \delta_e)}{T_m\pi\sigma + \delta_e}$$

is negative iff $\frac{\delta_e(T_m\alpha + s_E)}{d_E(T_m\pi\sigma + \delta_e)} < 1$. □

We did not attempt to analytically study the asymptotic stability of S_6^{noA}.

Stability analysis of the system with HBeAb. System (2.1) has the following non-negative equilibria: no liver, no CTLs

$$S_1 = \left(S_1^{noA}, 0, 0\right), \tag{5.7}$$

infection free state

$$S_2 = \left(S_2^{noA}, 0, 0\right), \tag{5.8}$$

no liver under CTL responses

$$S_3 = \left(S_3^{noA}, 0, 0\right), \tag{5.9}$$

clearance due to CTL responses

$$S_4 = \left(S_4^{noA}, 0, 0\right), \tag{5.10}$$

infection in the absence of any immune responses

$$S_5 = \left(S_5^{noA}, 0, 0\right), \tag{5.11}$$

infection during anergic CTL responses. There are up to four solutions of this form

$$S_6 = \left(S_6^{noA}, 0, 0\right). \tag{5.12}$$

S_1 through S_6 are the equilibria of (3.2) with additional variables $\bar{A} = 0$ and $\bar{X} = 0$.

Theorem 5.5. *Equilibria S_1 through S_4 are unstable.*

Proof. The Jacobian of system (2.1) evaluated at S_1 through S_4 has eigenvalue $\lambda_1 = s_A > 0$. Hence S_1 through S_4 are unstable equilibria. □

Theorem 5.6. *Equilibrium S_5 is locally asymptotically stable iff $\frac{\delta_e(T_m\alpha+s_E)}{d_E(T_m\pi\sigma+\delta_e)} < 1$ and $\frac{(c_X+k_m)(T_m s\pi+\delta_e s_A)}{T_m k_p c_X \pi} < 1$.*

Proof. Using *Maple* we find that the Jacobian of system (3.2) evaluated at S_5^{noA} has four eigenvalues $\lambda_1 = -r$, $\lambda_2 = -\delta_e$, $\lambda_3 = -c$, and $\lambda_4 = -\frac{T_m\beta p}{c}$ which are always negative. The remaining three eigenvalues are

$$\lambda_5 = \frac{\delta_e(T_m\alpha + s_E) - d_E(T_m\pi\sigma + \delta_e)}{T_m\pi\sigma + \delta_e},$$

which is negative iff $\frac{\delta_e(T_m\alpha+s_E)}{d_E(T_m\pi\sigma+\delta_e)} < 1$, and

$$\lambda_{6,7} = \frac{1}{2\delta_e}\Big[-(T_m\pi + (c_X + k_m)\delta_e - (T_m s\pi + \delta_e\alpha)) \pm \sqrt{(T_m\pi + (c_X + k_m)\delta_e - (T_m s\pi + \delta_e\alpha))^2 + 4\delta_e(s_A(c_X + k_m)\delta_e + \pi((s - k_p)c_X + sk_m)T_m)}\Big].$$

We find $Re(\lambda_{6,7}) < 0$ iff

$$\frac{T_m s\pi + \delta_e s_A}{T_m k_p\pi + \delta_e(c_X + k_m)} < 1, \tag{5.13}$$

and

$$\frac{(c_X + k_m)(T_m s\pi + \delta_e s_A)}{T_m k_p\pi} < 1. \tag{5.14}$$

We find that (5.14) implies (5.13), and hence all eigenvalues have negative real part and S_5 is locally asymptotically stable iff $\frac{\delta_e(T_m\alpha+s_E)}{d_E(T_m\pi\sigma+\delta_e)} < 1$ and $\frac{(c_X+k_m)(T_m s\pi+\delta_e s_A)}{T_m k_p c_X \pi} < 1$. □

Theorem 5.7. *If S_6^{noA} is unstable in system* (3.2)*, then S_6 is unstable in system* (2.1).

Proof. For S_6 the equilibrium levels of A and X are zero. When plugging $A = 0$ and $X = 0$ into the Jacobian, J, of system (2.1) yields

$$J = \begin{pmatrix} J^{noA} & (\star)^{5\times 2} \\ 0^{2\times 5} & \tilde{J} \end{pmatrix},$$

where J^{noA} is the Jacobian of system (3.2). Hence, if J^{noA} has an eigenvalue with positive real part, so does J. □

The remaining equilibria have an antibody response component. They are: no liver and maximal antibody responses

$$S_7 = \left(S_1^{noA}, A_m, 0\right), \tag{5.15}$$

infection free due to maximal antibody responses

$$S_8 = \left(S_2^{noA}, A_m, 0\right), \tag{5.16}$$

no liver under anergic CTLs and maximal antibody responses

$$S_9 = \left(S_3^{noA}, A_m, 0\right), \tag{5.17}$$

infection free due to combined CTLs and antibody responses

$$S_{10} = \left(S_4^{noA}, A_m, 0\right). \tag{5.18}$$

Theorem 5.8. *Equilibria S_7 and S_9 are unstable.*

Proof. The Jacobian of system (2.1) evaluated at S_7 or S_9 has eigenvalue $\lambda_1 = r > 0$. Hence S_7 and S_9 are unstable equilibria. □

Theorem 5.9. *Equilibrium S_8 is unstable.*

Proof. Using *Maple* we find that the Jacobian of system (2.1) evaluated at S_8 has eigenvalue

$$\lambda_1 = -\frac{c}{2} + \frac{\sqrt{4T_m\beta p + c^2}}{2},$$

which is always positive. Hence S_8 is an unstable equilibrium. □

Theorem 5.10. *Equilibrium S_{10} is locally asymptotically stable iff $s_E > d_E$ and $\frac{T_m\beta p s_E}{E_m\mu c(s_E - d_E)}$.*

Proof. Using *Maple* we find that the Jacobian of system (2.1) evaluated at S_{10} has two eigenvalues $\lambda_1 = -r$ and $\lambda_2 = -s_A$ which are always negative. A third eigenvalue $\lambda_3 = d_E - s_E$ is negative iff $s_E > d_E$. The remaining four eigenvalues are

$$\lambda_{4,5} = \frac{1}{2s_E}\left(-(cs_E + E_m\mu(s_e - d_E)) \pm \sqrt{(cs_E + E_m\mu(s_e - d_E))^2 + 4s_E(T_m\beta ps_E - E_m c\mu(s_E - d_E))}\right),$$

and

$$\lambda_{6,7} = \frac{1}{2}\left[-(A_m k_p + c_X + \delta_e + k_m) \pm \sqrt{(A_m k_p + c_X + \delta_e + k_m)^2 - 4((c_x + k_m)\delta_e + A_m c_X k_p)}\right]$$

If $s_E > d_E$, then $Re(\lambda_5),\ Re(\lambda_6),\ Re(\lambda_7) < 0$, and

$$Re(\lambda_4) < 0 \Longleftrightarrow \frac{T_m\beta ps_E + E_m c d_E\mu}{E_m c\mu s_E} < 1 \Longleftrightarrow \frac{T_m\beta ps_E}{E_m c\mu(s_E - d_E)} < 1.$$

□

Infection with no CTLs and positive antibody responses includes up to two states, given by

$$S_{11} = \left(0, T_m, \frac{T_m p}{c}, \bar{e}, 0, \frac{A_m((s(c_X + k_m) - k_p c_X)\bar{e} + s_A(c_X + k_m))}{(s\bar{e} + s_A)(c_X + k_m)}, \frac{T_m\pi - \delta_e\bar{e}}{c_X}\right), \tag{5.19}$$

where $\bar{e}$ satisfies the quadratic equation $C_2\bar{e}^2 + C_1\bar{e} + C_0 = 0$ with

$$\begin{aligned}
C_2 &= \left(((-k_p A_m - \delta_e)s + A_m k_p^2)c_X^2 - sk_m(k_p A_m + 2\delta_e)c_X - \delta_e k_m^2 s\right)/(c_X + k_m)^2,\\
C_1 &= \left(((-k_p A_m - \delta_e)s_A + sT_m\pi)c_X + k_m(sT_m\pi - \delta_e s_A)\right)/(c_X + k_m),\\
C_0 &= T_m\pi s_A.
\end{aligned}$$

We did not attempt to analytically study the asymptotic stability of S_{11}

Lastly, infection during anergic CTLs and inefficient antibody responses is given by:

$$S_{12} = \left(\bar{T}(\bar{y}), \bar{I}(\bar{y}), \bar{V}(\bar{y}), \bar{e}(\bar{y}), \bar{E}(\bar{y}), \bar{A}(\bar{y}), \bar{X}(\bar{y})\right), \tag{5.20}$$

where

$$\begin{aligned}
\bar{T}(\bar{y}) = \Bigg[& E_m(((((A_m k_p + \delta_e)\alpha - \pi d_E\sigma)s - A_m\alpha k_p^2)c_X^2 - 2sk_m((-\frac{A_m k_p}{2} - \delta_e)\alpha + \pi d_E\sigma)c_X - sk_m^2(\pi d_E\sigma - \alpha\delta_e))\bar{y}^2\\
& + ((\pi(s_E - d_E)s - s_A((-A_m k_p + \delta_e)\alpha + pid_E\sigma))c_X - (-pi(s_E - d_E)s + s_A(\pi d_E\sigma - \alpha\delta_e))k_m)\bar{y}\\
& + \pi s_A(s_E - d_E)c\mu\Bigg] \times \Bigg[((\alpha(((A_m k_p + \delta_e)s - A_m k_p^2)c_X^2 + sk_m(A_m k_p + 2\delta_e)c_X + \delta_e k_m^2 s)\bar{y}^2\\
& + ((\pi s_E s + s_A\alpha(A_m k_p + \delta_E))c_X + k_m(\alpha\delta_e s_A + \pi s_E s))\bar{y} + s_E s_A\pi)p\beta\Bigg]^{-1},
\end{aligned}$$

$$\begin{aligned}
\bar{I}(\bar{y}) = & \left[((((A_m k_p + \delta_e)s - A_m k_p^2)c_X^2 + sk_m(A_m k_p + 2\delta_e)c_X + \delta_e k_m^2 s)\bar{y} + ((A_m k_p + \delta_e)c_X + \delta_e k_m)s_A)\bar{y}\right]\\
& \times \left[\pi((c_X + k_m)s\bar{y} + s_A)\right]^{-1}
\end{aligned}$$

$$\bar{V}(\bar{y}) = \frac{p}{c}\bar{I}(\bar{y}),$$

$$\bar{e}(\bar{y}) = (c_x + k_m)\bar{y},$$

$$\begin{aligned}\bar{E}(\bar{y}) = \Big[&((((A_m k_p + \delta_e)\alpha - \pi d_E\sigma)s - A_m\alpha k_p^2)c_X^2 + ((A_m k_p + 2\delta_e)\alpha - 2\pi d_E\sigma)k_m s c_X + k_m s(-\pi d_E\sigma + \alpha\delta_e))\bar{y}^2 \\ &+ ((\pi(s_E - d_E)s + s_A((A_m k_p + \delta_e)\alpha - \pi d_E\sigma))c_X + k_m(\pi(s_E - d_E)s + s_A(-\pi d_E\sigma + \alpha\delta_e)))\bar{y} \\ &+ \pi s_A(s_E - d_E)E_m\Big] \times \Big[\alpha(((A_m k_p + \delta_e)s - A_m k_p^2)c_X^2 + s k_m(A_m k_p + 2\delta_e)c_X + \delta_e k_m^2 s)\bar{y}^2 \\ &+ ((\pi s_E s + s_A\alpha(A_m k_p + \delta_e))c_X + k_m(\alpha\delta_e s_A + \pi s_E s))\bar{y} + s_E s_A\pi\Big]^{-1},\end{aligned}$$

$$\bar{A}(\bar{y}) = \frac{A_m((s(c_X + k_m) - k_p c_X)\bar{y} + s_A)}{(c_X + k_m)s\bar{y} + s_A},$$

$$\bar{X}(\bar{y}) = \frac{A_m k_p\bar{y}((s(c_X + k_m) - k_p c_X)\bar{y} + s_A)}{(c_X + k_m)s\bar{y} + s_A},$$

and $\bar{y}$ is the root of a degree seven polynomial whose expression is messy and will not be provided here (*Maple* file available upon request). We did not attempt to analytically study the asymptotic stability of S_{12}.

Appendix 2. Stability analysis of the system with mutations. We determine system (3.6)'s equilibria and their stability under the assumption that $\beta_m = \beta_w = \beta$, $\mu_m = \mu_w = \mu$, $p_m = p_w = p$, and $c_m = c_w = c$. System (3.6) has the following non-negative equilibria.

$$S_1^{mut} = (0, 0, 0, 0, 0, 0, 0, 0, 0, 0)\,, \tag{5.21}$$

$$S_2^{mut} = (T_m, 0, 0, 0, 0, 0, 0, 0, 0, 0)\,, \tag{5.22}$$

$$S_3^{mut} = \left(0, 0, 0, 0, 0, 0, \frac{E_m(s_E - d_E)}{s_E}, 0, 0\right), \tag{5.23}$$

$$S_4^{mut} = \left(T_m, 0, 0, 0, 0, 0, \frac{E_m(s_E - d_E)}{s_E}, 0, 0\right), \tag{5.24}$$

$$S_5^{mut} = (0, 0, 0, 0, 0, 0, 0, A_m, 0)\,, \tag{5.25}$$

$$S_6^{mut} = (T_m, 0, 0, 0, 0, 0, 0, A_m, 0)\,, \tag{5.26}$$

$$S_7^{mut} = \left(0, 0, 0, 0, 0, 0, \frac{E_m(s_E - d_E)}{s_E}, A_m, 0\right), \tag{5.27}$$

$$S_8^{mut} = \left(T_m, 0, 0, 0, 0, 0, \frac{E_m(s_E - d_E)}{s_E}, A_m, 0\right), \tag{5.28}$$

$$S_9^{mut} = \left(0, \frac{\delta_e}{\pi}e, T_m - \frac{\delta_e}{\pi}e, \frac{p(1-\Phi)\delta_e}{c\pi}e, \frac{T_m p}{c} - \frac{p(1-\Phi)\delta_e}{c\pi}e, e, 0, 0, 0\right), \tag{5.29}$$

where e can take on any value less than or equal to $\frac{T_m\pi}{\delta_e}$ (for biological relevance, i.e. non-negativity).

$$S_{10}^{mut} = \left(0, \bar{I}_w(e), T_m - \bar{I}_w(e), \frac{p(1-\Phi)}{c}\bar{I}_w(e), \frac{p}{c}(T_m - (1-\Phi)\bar{I}_w(e)), e, 0, \bar{A}(e), \bar{X}(e)\right), \tag{5.30}$$

where e can take on any value, and

$$\begin{aligned}\bar{I}_w(e) &= ((((s\delta_e \\ &= k_p A_m(s-k_p))e + s_A(k_p A_m + \delta_e))c_X^2 + k_m(k_p A_m + 2\delta_e)(es+s_A)c_X + k_m^2\delta_e(es+s_A))e) \\ &\quad \times (\pi(c_X+k_m)^2(es+s_A))^{-1},\end{aligned}$$

$$\bar{A}(e) = \frac{A_m(((s-k_p)e+s_A)c_X + k_m(es+s_A))}{(es+s_A)(c_X+k_m)},$$

$$\bar{X}(e) = \frac{k_p A_m(((s-k_p)c_X + sk_m)e + s_A(c_X+k_m))e}{(c_X+k_m)^2(es+s_A)}.$$

$$S_{11}^{mut} = \left(\frac{E_m\mu c(\alpha\bar{I}_n + s_E - d_E)}{\beta p(\alpha\bar{I}_n + s_E)}, 0, \bar{I}_n, 0, \frac{p}{c}\bar{I}_n, 0, \frac{E_m(\alpha\bar{I}_n + s_E - d_E)}{\alpha\bar{I}_n + s_E}, 0, 0\right), \tag{5.31}$$

where $\bar{I}_n$ is a root of the fourth degree polynomial

$$C_4\bar{I}^4 + C_3\bar{I}^3 + C_2\bar{I}^2 + C_1\bar{I} + C_0,$$

with

$$C_4 = \alpha^2\beta^2p^2r,$$

$$C_3 = 2\alpha((-\frac{\beta T_m(-E_m\mu + r)p}{2} + c\mu r E_m)\alpha + \beta r p s_E)\beta p,$$

$$C_2 = cr\mu E_m(cE_m\mu - p\beta T_m)\alpha^2 + 2(-(-mu(s_E - \frac{d_E}{2})E_m + rs_E)\beta T_m p + cr\mu E_m(2s_E - d_E))\beta p\alpha + \beta^2p^2rs_E^2,$$

$$C_1 = 2c^2\alpha r\mu^2(s_E - d_E)E_m^2 - 2\mu\beta p(-\frac{\beta T_m s_E(s_E-d_E)p}{2} + (-s_E^2 + (T_m\alpha + d_E)s_E - \frac{\alpha T_m d_E}{2})cr)E_m - T_m\beta^2p^2rs_E^2,$$

$$C_0 = \mu E_m c(c\mu(s_E - d_E)E_m - T_m\beta p s_E)r(s_E - d_E).$$

$$S_{12}^{mut} = \left(\frac{E_m\mu c(\alpha\bar{I}_n + s_E - d_E)}{\beta p(\alpha\bar{I}_n + s_E)}, 0, \bar{I}_n, 0, \frac{p}{c}\bar{I}_n, 0, \frac{E_m(\alpha\bar{I}_n + s_E - d_E)}{\alpha\bar{I}_n + s_E}, A_m, 0\right), \tag{5.32}$$

where $\bar{I}_n$ is defined as in S_{11}^{mut}.

Theorem 5.11. *Equilibria $S_1^{mut} - S_7^{mut}$, and S_{11}^{mut} are unstable.*

Proof. The Jacobian of system (3.6) evaluated at S_1^{mut}, S_3^{mut}, S_5^{mut}, and S_7^{mut} has eigenvalue $\lambda_1 = r > 0$. The Jacobian of system (3.6) evaluated at S_2^{mut}, S_4^{mut}, and S_{11}^{mut} has eigenvalue $\lambda_1 = s_A > 0$. The Jacobian of system (3.6) evaluated at S_6^{mut} has eigenvalue $\lambda_1 = -\frac{c}{2} + \frac{\sqrt{4T_m\beta p + c^2}}{2} > 0$. Thus, $S_1^{mut} - S_7^{mut}$, and S_{11}^{mut} are unstable equilibria. □

Theorem 5.12. *Equilibrium S_8^{mut} is locally asymptotically stable iff $s_E > d_E$ and $\frac{T_m\beta p s_E}{E_m\mu c(s_E - d_E)} < 1$.*

Proof. Using *Maple* we find that the Jacobian of system (3.6) evaluated at S_8^{mut} has two eigenvalues $\lambda_1 = -r$ and $\lambda_2 = -s_A$ which are always negative. A third eigenvalue $\lambda_3 = d_E - s_E$ is negative iff $s_E > d_E$. The remaining six eigenvalues are

$$\lambda_{4,5} = \frac{1}{2s_E}\left(-(cs_E + E_m\mu(s_e - d_E)) \pm \sqrt{(cs_E + E_m\mu(s_e - d_E))^2 + 4s_E(T_m\beta p s_E - E_m c\mu(s_E - d_E))}\right),$$

$$\lambda_{6,7} = \frac{1}{2s_E}\left(-(cs_E + E_m\mu(s_e - d_E)) \pm \sqrt{(cs_E + E_m\mu(s_e - d_E))^2 + 4s_E(T_m\beta p(1-\Phi) s_E - E_m c\mu(s_E - d_E))}\right),$$

and

$$\lambda_{8,9} = \frac{1}{2}\left[-(A_m k_p + c_X + \delta_e + k_m) \pm \sqrt{(A_m k_p + c_X + \delta_e + k_m)^2 - 4((c_x + k_m)\delta_e + A_m c_X k_p)}\right]$$

If $\lambda_3 < 0$, *i.e.* $s_E > d_E$, then $-(cs_E + E_m\mu(s_e - d_E)) < 0$ and hence $Re(\lambda_5), Re(\lambda_7) < 0$. Further $Re(\lambda_8), Re(\lambda_9) < 0$, and

$$Re(\lambda_4) < 0 \iff \lambda_4 < 0 \iff \frac{T_m\beta p s_E}{E_m\mu c(s_E - d_E)} < 1,$$
$$Re(\lambda_6) < 0 \iff \lambda_6 < 0 \iff \frac{T_m\beta p(1-\Phi) s_E}{E_m\mu c(s_E - d_E)} < 1.$$

Since $\Phi \geq 0$, if $Re(\lambda_4) < 0$ then $Re(\lambda_6) < 0$. Hence all eigenvalues have negative real part and S_8^{mut} is locally asymptotically stable iff $s_E > d_E$ and $\frac{T_m\beta p s_E}{E_m\mu c(s_E - d_E)} < 1$. □

Proving stability for S_9^{mut}, S_{10}^{mut}, and S_{12}^{mut} is messy and will not be presented here.

Appendix 3. Sensitivity Analysis. We analyzed the time-dependent semi-relative sensitivity of model (2.1)'s dynamics to small changes in various parameters. For times 0 to 2 years and parameters $P = \{\alpha, A_m, \beta, k_p, \mu, \pi, s, s_A, s_E, \sigma\}$ we look at the semi-relative sensitivity curves $P\frac{\partial Y}{\partial P}$, where $Y = \{T, I, V, e, E, A, X\}$. The results are presented below. As expected, we find that $\{\alpha, A_m, \mu, s, s_A, s_E\}$ have negative effects on $\{I, V, e\}$ and positive effects on E (see Figures S2, S3, S6, S8, S9, S10), while $\{\beta, k_p, \pi, \sigma\}$ have the opposite effects (see Figures S4, S5, S7, S11). Furthermore, we observe that

virus, HBeAg, and effector cell populations are most sensitive to changes in k_p and s (see Figures S12–S14, left panel). While HBeAg and effector cells are most sensitive around day 125 regardless of the parameter, the maximal sensitivity of the virus population to β, A_m and μ occurs later (see Figures S12–S14, right panel).

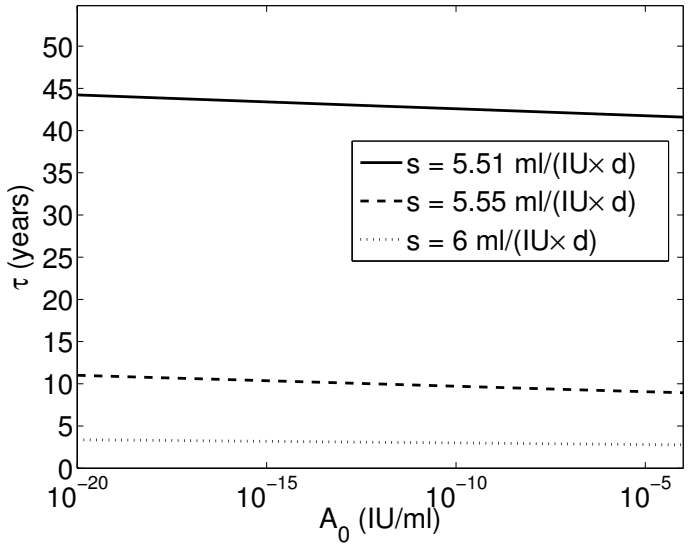

Figure S1. Time to HBeAg seroclearance versus initial HBeAb level A_0 for different HBeAg production rates s.

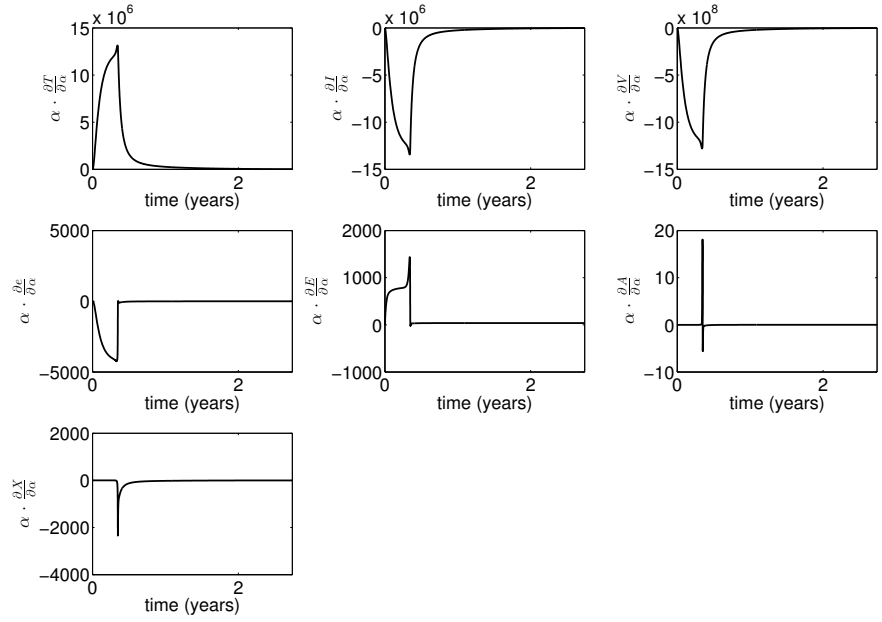

Figure S2. Semi-relative sensitivity curves for the infected cell dependent immune cell activation rate α.

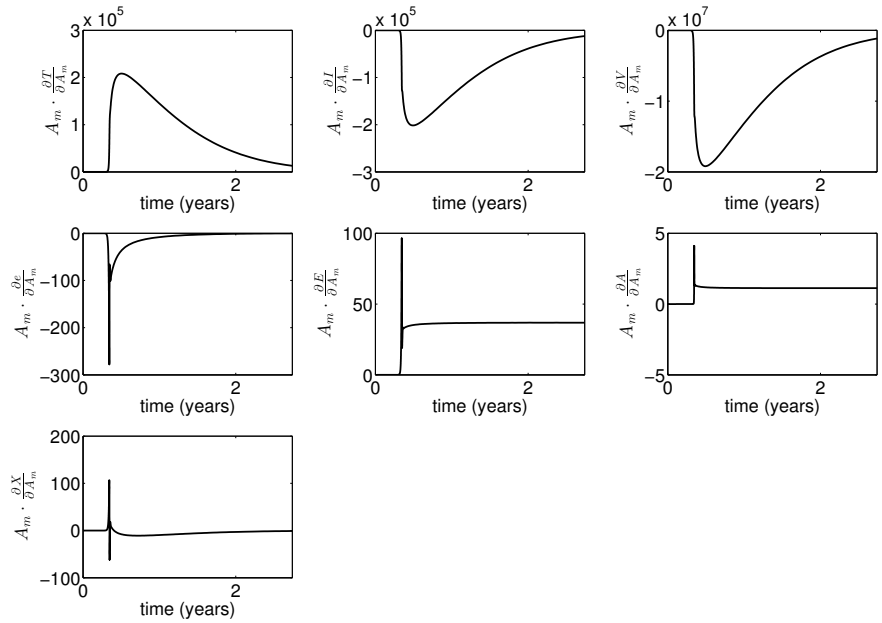

Figure S3. Semi-relative sensitivity curves for the antibody carrying capacity A_m.

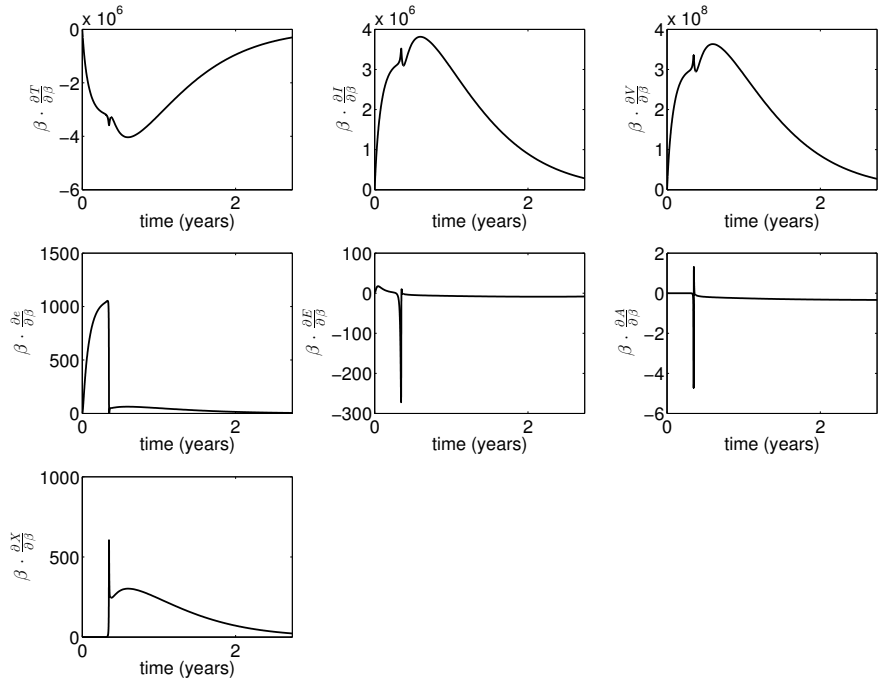

Figure S4. Semi-relative sensitivity curves for the viral infectivity rate β.

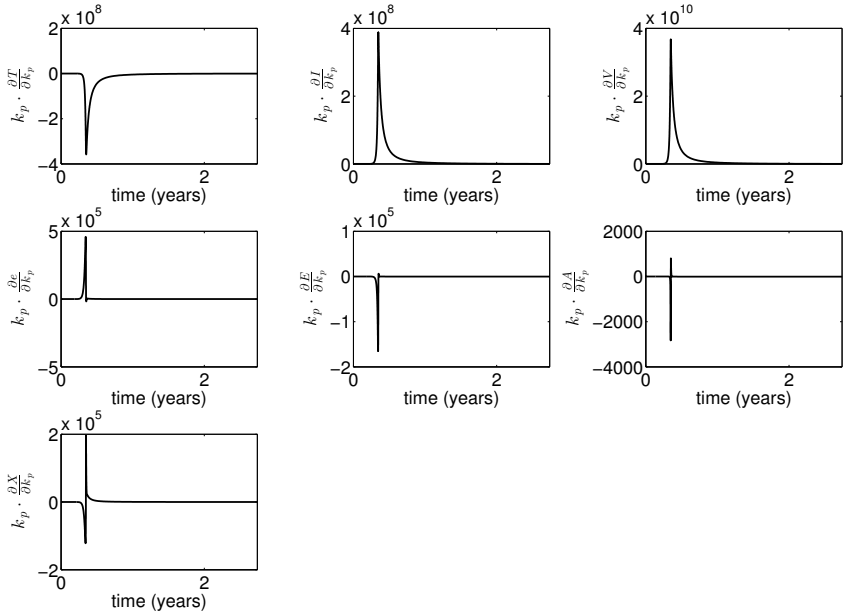

Figure S5. Semi-relative sensitivity curves for the immune complex binding rate k_p.

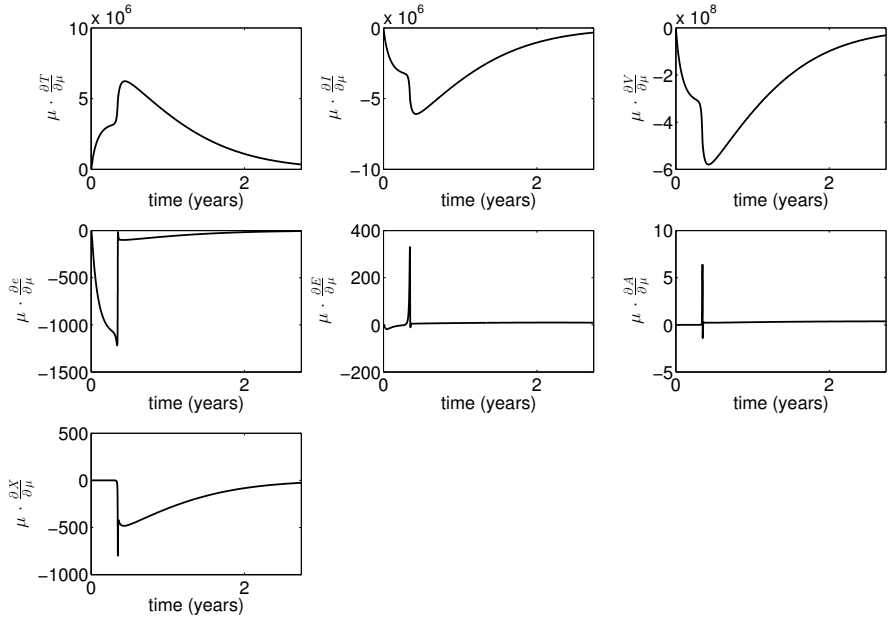

Figure S6. Semi-relative sensitivity curves for the immune mediated clearance rate of infected cells μ.

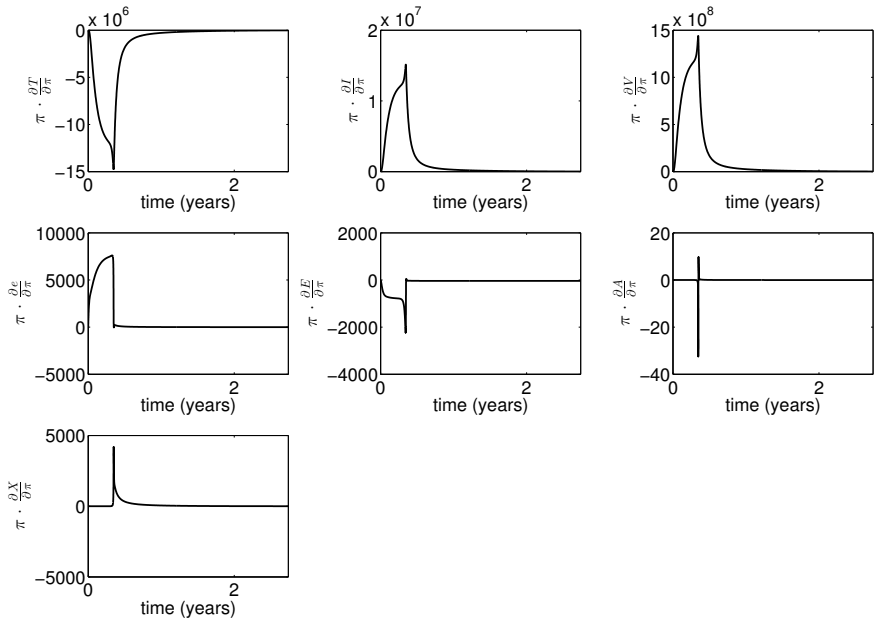

Figure S7. Semi-relative sensitivity curves for the HBeAg production rate π.

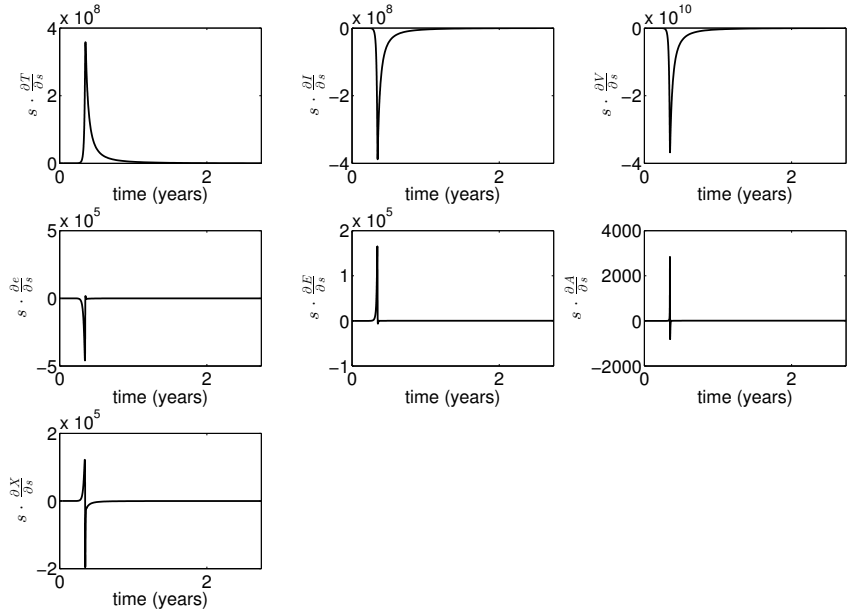

Figure S8. Semi-relative sensitivity curves for the HBeAg dependent HBeAb production rate s.

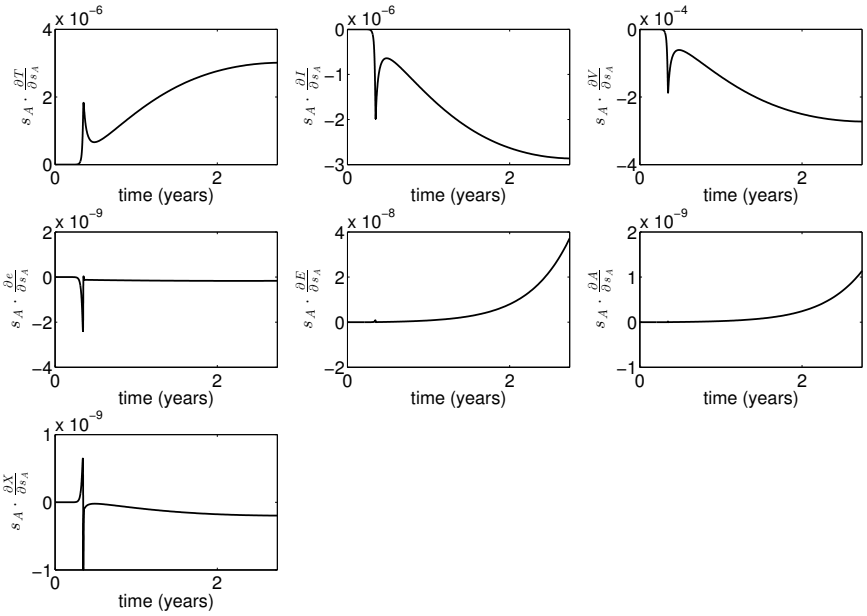

Figure S9. Semi-relative sensitivity curves for the HBeAg independent HBeAb production rate s_A.

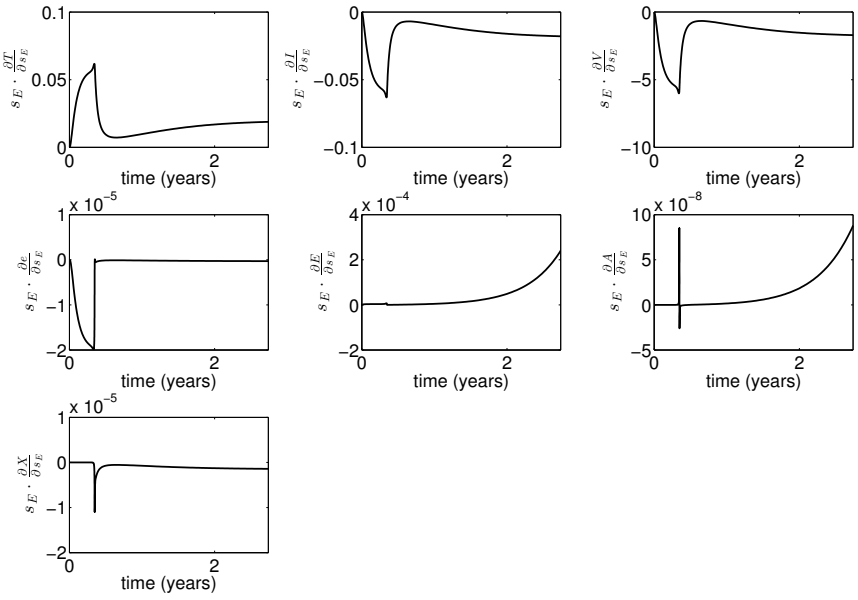

Figure S10. Semi-relative sensitivity curves for the infected cell independent immune cell activation rate s_E.

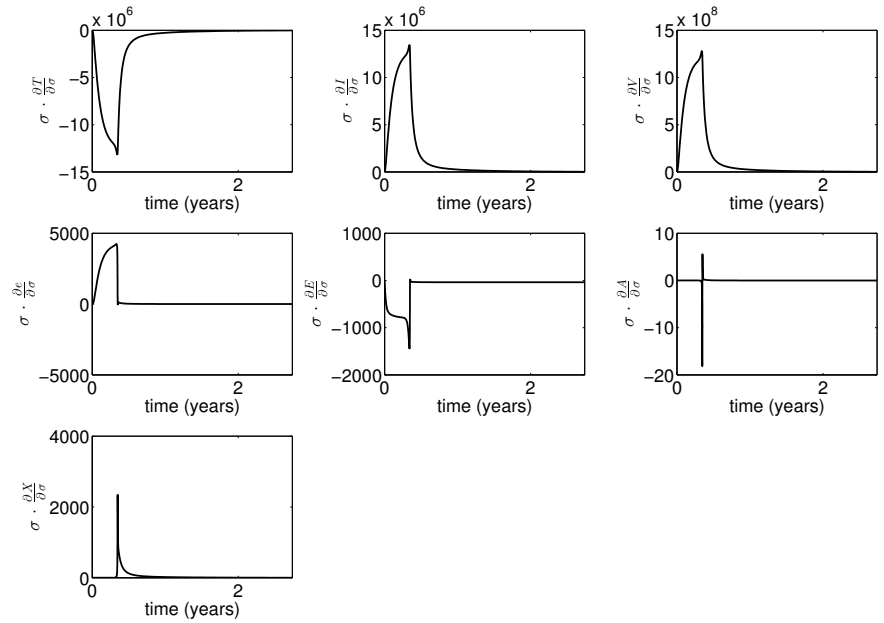

Figure S11. Semi-relative sensitivity curves for the inhibitory strength of HBeAg on CTLs σ.

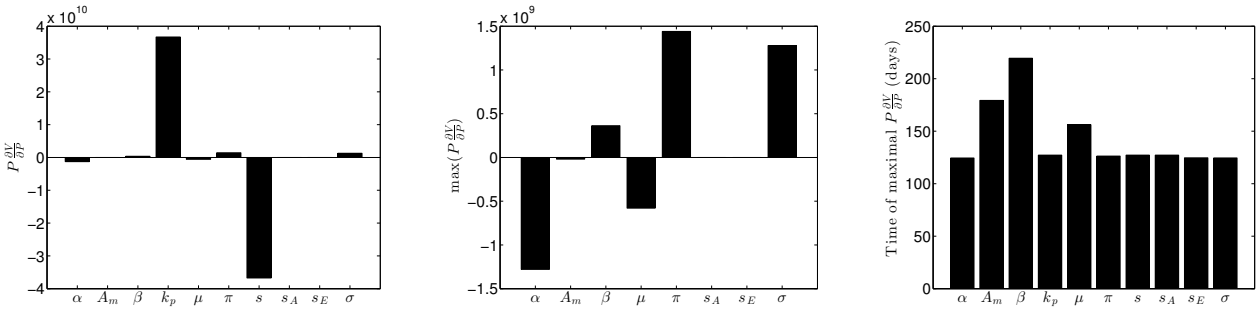

Figure S12. (Left and center) Maximal sensitivity of virus population on parameters during the first two years. (Right) Time when sensitivity is maximal.

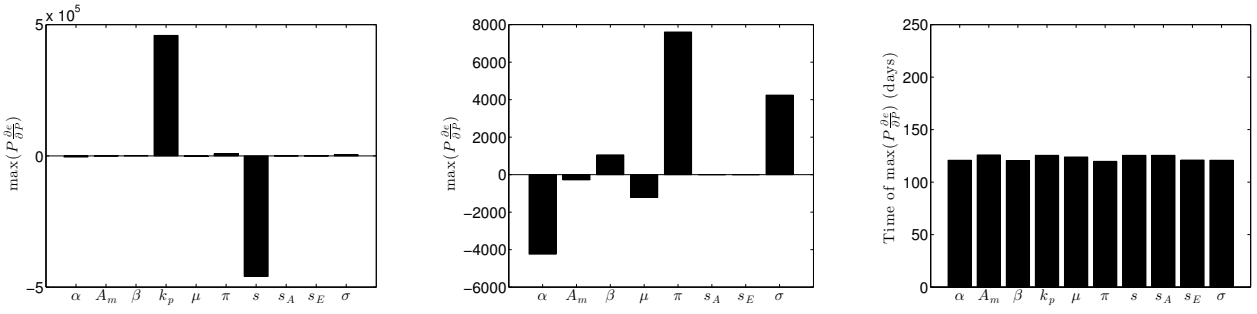

Figure S13. (Left and center) Maximal sensitivity of HBeAg population on parameters during the first two years. (Right) Time when sensitivity is maximal.

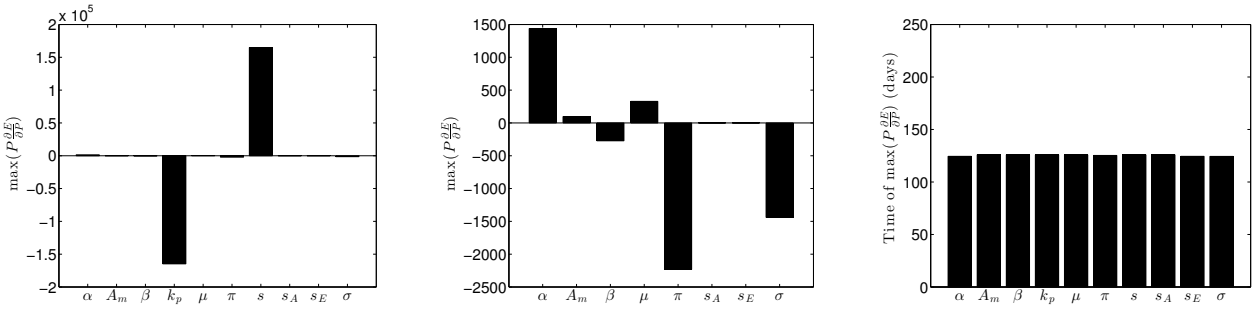

Figure S14. (Left and center) Maximal sensitivity of effector cell population on parameters during the first two years. (Right) Time when sensitivity is maximal.

Heterogeneity in infected and virus populations. Studies have reported different half-lives for the wildtype and mutant virus strains, although the exact values vary. Dandri *et al.* reported average half-lives of 46 and 2.5 minutes, corresponding to 20-fold higher clearance rate of mutant compared to wildt-ype strains [76]. Ribeiro *et al.* reported half-lives of 25.2 and 13.1 hours, corresponding to 2-fold increase in clearance of mutant compared to wildtype virus [77]. Moreover, Ribeiro *et al.*, reported shorter half-lives of cells infected by mutant compared to wildtype virus, 12.1 days versus 16 days (a 1.3-fold increase in the clearance rate of I_m compared with I_w) [77]. In this study we assumed that both viruses have half-lives of 4 hours, corresponding to the clearance rates $c_w = c_m = 4.2$/day and both infected cell types are removed (by the effector cells) at rate μ. To address how differences in the two strains half-lives affect our results, we change their clearance rates as follows: we keep $c_w = 4.2$/day, and assume a 10-fold increase in the mutant clearance, $c_m = 42$/day, corresponding to 24 minutes half-life. Moreover, we keep the killing rate of the cells infected with the wildtype virus at $\mu_w = \mu = 6\times10^{-5}$ and increase $\mu_m = 1.3 \times \mu = 8 \times 10^{-5}$, corresponding to half-lives of 11.5 and 8.7 days under maximal CTL response E_m. Lastly, it has been suggested that cells that express mutant virus can lose the ability to express wildtype virus [78]. This can be modeled by assuming that a fraction z of cells infected with the wildtype virus transitions into the population of cells infected with the mutant virus. The system of equations expressing these changes is

$$
\begin{aligned}
\frac{dT}{dt} &= r(T + I_w + I_m)\left(1 - \frac{T + I_w + I_m}{T_m}\right) - \beta(TV_w - TV_m),\\
\frac{dI_w}{dt} &= \beta TV_w - \mu_w I_w E - zI_w,\\
\frac{dI_m}{dt} &= \beta TV_m - \mu_m I_m E + zI_w,\\
\frac{dV_w}{dt} &= p_w(1 - \Phi(t))I_w - c_w V_w,\\
\frac{dV_m}{dt} &= p_m I_m + p_w \Phi(t) I_w - c_m V_m,\\
\frac{de}{dt} &= \pi I_w - \delta_e e - k_p A e + k_m X,\\
\frac{dE}{dt} &= \frac{s_E E + \alpha(I_w + I_m)E}{1 + \sigma e}\left(1 - \frac{E}{E_m}\right) - d_E E,\\
\frac{dA}{dt} &= (s_A A + seA)\left(1 - \frac{A}{A_m}\right) - k_p A e + k_m X,\\
\frac{dX}{dt} &= k_p A e - k_m X - c_X X.
\end{aligned}
\tag{S1}
$$

We solved the model for four parameter combinations: (i) $\Phi = 0.1$, $z = 0$, $c_w = c_m$, $\mu_w = \mu_m$; (ii) $\Phi = 0.1$, $z = 0$, $c_w < c_m$, $\mu_w < \mu_m$; (iii) $\Phi = 0.1$, $z \neq 0$, $c_w = c_m$, $\mu_w = \mu_m$; (iv) $\Phi = 0.1$, $z \neq 0$, $c_w < c_m$, $\mu_w < \mu_m$. We predict the longest time to HBeAg seroclearance in case (ii), when cells infected by the wildtype keep their ability to produce wildtype virus ($z = 0$), and the mutant families V_m and I_m have faster clearance rates (10 and 1.3-fold increase, respectively) (see Figure S15, solid lines). When a fraction $z = 0.01$ of cells infected with the wildtype transition into cells producing only mutant virus (cases iii and iv), we obtain faster HBeAg seroclearance times (see Figure S15, dashed and dotted lines). As before, however, increasing the mutant virus and cells infected with mutant virus clearance rates (case iv), decreases the overall HBeAg seroclearance time (see Figure S15, dotted lines). Interestingly, the dynamics of the model now allow for long-term coexistence between the mutant and wildtype virus strains.

We next investigate how these results change if we vary Φ and z. We let $\tau_{same}(z, \Phi)$ be the time to HBeAg seroclearance assuming equal clearance rates for wildtype and mutant populations, $\tau_{diff}(z, \Phi)$ be the time to HBeAg seroclearance assuming a 10 and 1.3 fold increased clearance rate of mutant virus and cells infected with the mutant virus, and

$$
HL(z, \Phi) = \left(\int_0^{\tau(z,\Phi)} \left(\mu_w \frac{I_w(t)}{T_m} E(t) + \mu_m \frac{I_m(t)}{T_m} E(t)\right) dt\right) / \tau(z, \Phi),
$$

be the average monthly hepatocyte turnover. Here τ is either τ_{same} or τ_{diff}. Note, that we assume that mutations, transitions, and HBeAb formation all start concomitantly at time $t = 0$. We find that for all $10^{-4} < z < 10^{-1}$ and $10^{-2} < \Phi < 1$, the 10 and 1.3-fold increases in clearance rates of mutant virus and cells infected with mutant virus result in slower HBeAg clearance ($\tau_{same}(z, \Phi) - \tau_{diff}(z, \Phi) < 0$ in Figure S16, left panel), but decreased monthly hepatocyte turnover ($HL_{same}(z, \Phi) - HL_{diff}(z, \Phi) > 0$, in

Figure S16, right panel). Furthermore, the negative impact that increased mutant clearance rates have on the time to HBeAg seroclearance is most prevalent for intermediate fractions of mutations Φ and intermediate transition rates z (see Figure S15, left panel, blue region).

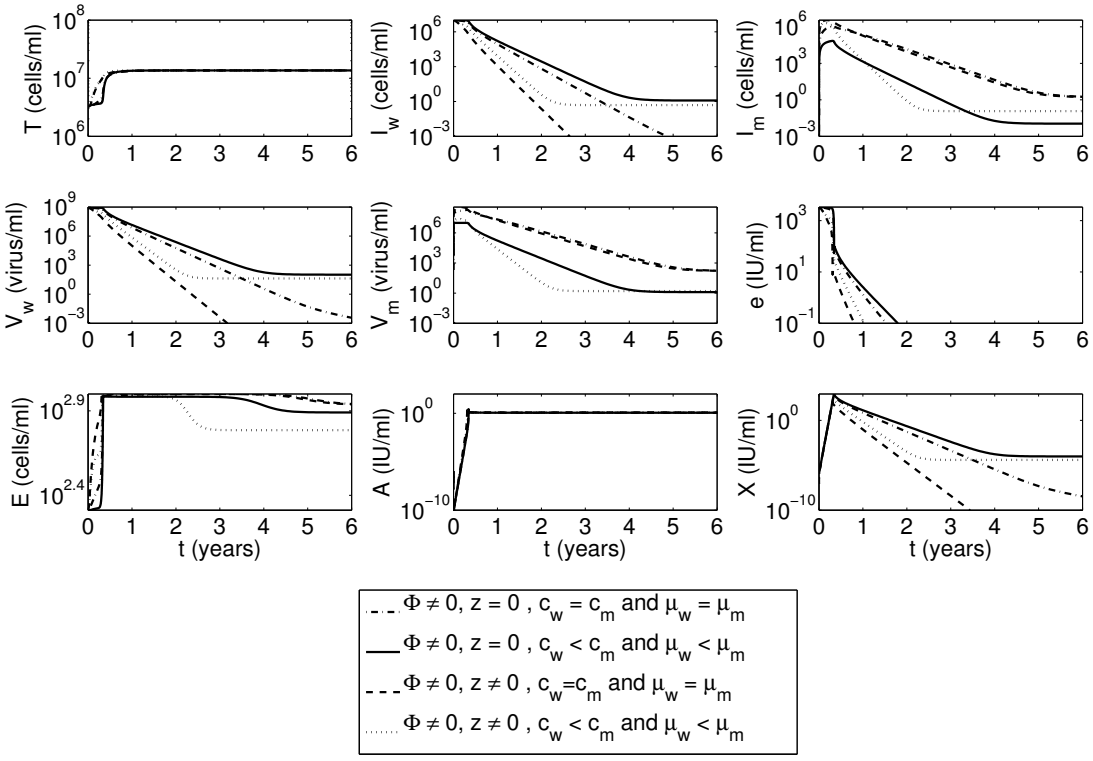

Figure S15. Dynamics of system (S1) when a fraction $\Phi = 0.1$ of produced virions has core/precore mutations in the absence of transition from I_w to I_m for equal clearance rates of wildtype and mutant virus and wildtye and mutant infected cell (dash-dotted curves), and for increased clearance of mutant virus and mutant infected cells (solid curves); and in the presence of transition from I_w to I_m at rate $z = 0.01$ with equal clearance rates (dashed) curves, and different clearance rates (dotted curves).

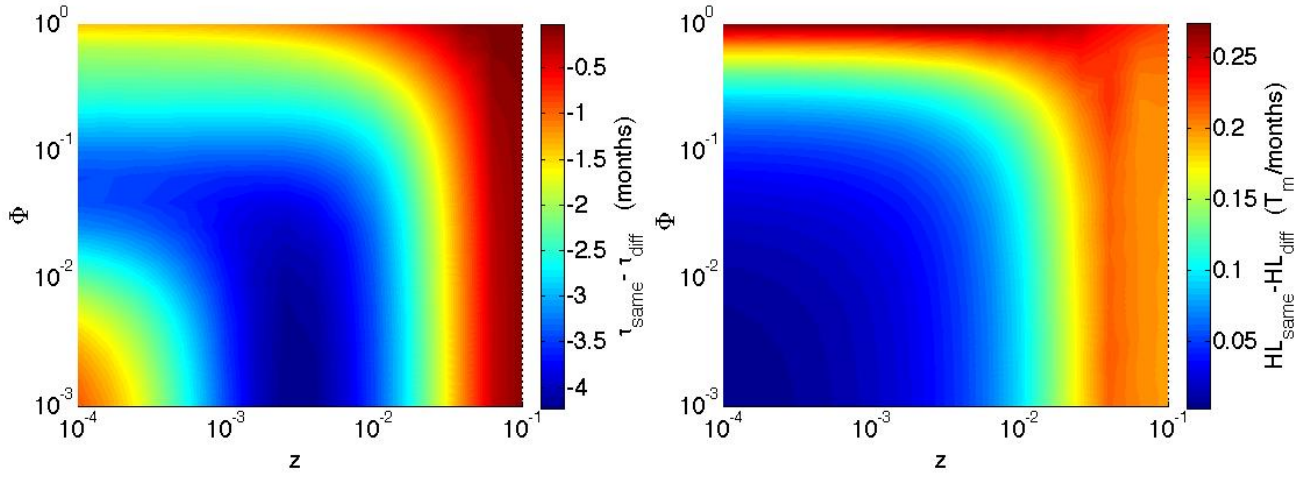

Figure S16. (Left) Heatmap for the difference in times to HBeAg seroclearance if clearance rates for wildtype and mutant populations are the same or if clearance rates for mutant populations are increased (10 fold for virus and 1.3 fold for infected cells), versus the fraction z of infected cells transitioning from I_w into I_m and the fraction Φ of virions produced by wildtype infected cells that are mutant. (Right) Heatmap for the difference in monthly hepatocyte turnover under equal clearance rates or increased mutant clearance rates.